Global warming and acid atmospheric deposition impacts on carbonate dissolution and CO2 fluxes in French karst hydrosystems: evidence from hydrochemical monitoring in recent decades

Stéphane Binet, J.L. Probst, Christelle Batiot-Guilhe, J.L. Seidel, C. Emblanch, N. Peyraube, Jean-Baptiste Charlier, M. Bakalowicz, Anne Probst

▶ **To cite this version:**

HAL Id: hal-02387529
https://hal.science/hal-02387529

Submitted on 3 Dec 2019

Global warming and acid atmospheric deposition impacts on carbonate dissolution and CO2 fluxes in French karst hydrosystems: evidence from hydrochemical monitoring in recent decades

Stéphane Binet, J.L. Probst, C. Batiot, J.L. Seidel, C. Emblanch, N. Peyraube, J.B. Charlier, M. Bakalowicz, Anne Probst

HAL Id: hal-02387529
https://hal.archives-ouvertes.fr/hal-02387529

Submitted on 3 Dec 2019

Journal Pre-proofs

Global warming and acid atmospheric deposition impacts on carbonate dissolution and CO_2 fluxes in French karst hydrosystems: evidence from hydrochemical monitoring in recent decades

S. Binet, J.L. Probst, C. Batiot, J.L. Seidel, C. Emblanch, N. Peyraube, J.B. Charlier, M. Bakalowicz, A. Probst

Please cite this article as: Binet, S., Probst, J.L., Batiot, C., Seidel, J.L., Emblanch, C., Peyraube, N., Charlier, J.B., Bakalowicz, M., Probst, A., Global warming and acid atmospheric deposition impacts on carbonate dissolution and CO_2 fluxes in French karst hydrosystems: evidence from hydrochemical monitoring in recent decades, *Geochimica et Cosmochimica Acta* (2019), doi: https://doi.org/10.1016/j.gca.2019.11.021

Global warming and acid atmospheric deposition impacts on carbonate dissolution and CO_2 fluxes in French karst hydrosystems: evidence from hydrochemical monitoring in recent decades.

Binet S.[1,2], Probst J.L. [1], Batiot C. [3], Seidel J.L. [3], Emblanch C. [4], Peyraube N. [5], Charlier J.B. [6], Bakalowicz M. [3], Probst A [1].

(1) EcoLab, Université de Toulouse, CNRS, UPS, Toulouse INP, Toulouse, France

(2) ISTO, Université d'Orléans, CNRS, BRGM, OSUC, France

(3) HSM, Université de Montpellier, France

(4) EMMAH, Université d'Avignon pays de Vaucluse, INRA, France

(5) Université de Bordeaux, France.

(6) BRGM, Université de Montpellier, France

ABSTRACT:

The long-term change in surface water chemistry over time in remote areas is usually related to global change, including several processes such as global warming and acid atmospheric pollution. These cumulative factors limit the quantitative interpretation of the global warming effect on surface water acidification in relation to the atmospheric CO_2 sink. To quantitatively estimate the impact of global warming on the atmospheric/soil CO_2 uptake by carbonate weathering, the approach proposed here involves discriminating the proportion of [Ca+Mg] in waters resulting from soil carbonic acid dissolution (equal to the amount of CO_2 uptake from soil / atmosphere) from the proportion resulting from strong acid pollution. This approach was applied to 5 karst hydrosystems located in France, far from local pollution sources and with several decades of hydrochemical monitoring.

 [Ca+Mg] from acid deposition represented between 16 and 25% of the total [Ca+Mg] concentration and the flux was positively correlated with the atmospheric deposition flux. This [Ca+Mg] increase is associated with increasing [Mg] and was found to be driven by the acid pollution inputs.

Equilibrating water with calcite in presence of carbonic acid will release [Ca+Mg] into solution. The input of strong acids from atmospheric pollution contributes more to magnesian calcite dissolution because its solubility is lower than that of calcite.

Since the 1980s, the decrease in [Ca+Mg] production due to the decrease in acid atmospheric deposition has minimized the increase in [Ca+Mg] linked to CO_2 partial pressure (pCO_2) increasing with global warming. It was found that [Ca+Mg] from H_2CO_3 dissolution did not decrease with an increase in air temperature, as suggested by carbonate solubility. The annual fluxes of Ca+Mg from H_2CO_3 dissolution, calculated for an average flow, showed a positive gradient with air temperature, of about 0.061 $mol.m^2.yr^{-1}°C^{-1}$ (±0.006). In low rainfall areas, the pCO_2 increase with air temperature was stronger than in rainy areas. For an average specific discharge of 300 $L.m^{-2}yr^{-1}$, global warming is estimated to increase the CO_2 uptake flux by about 204 micromol$.L^{-1}.°C^{-1}$ (5.7% of the observed flux).

1. INTRODUCTION

The atmospheric/soil CO_2 captured by vegetation and released in soils by organic matter mineralization contributes to producing carbonic acid in soil solutions. Carbonic acid is the main natural driver of the chemical weathering of rocks. Weathering mineralizes C from the atmosphere/soil that is dissolved and partially exported towards the oceans. At the global scale, carbonate dissolution consumes 0.38 $Gt.yr^{-1}$ of atmospheric/soil CO_2, i.e. 0.1 Gt $C.yr^{-1}$ (Liu and Zhao, 1999; Amiotte Suchet et al., 2003). The dissolution of carbonate consumes 40% of the total CO_2 uptake by continental weathering and releases 0.21 $Gt.yr^{-1}$ of dissolved inorganic carbon (DIC) into the oceans of which 50% (equation 1) originates from atmospheric/soil CO_2 (Amiotte Suchet et al., 2003).

$[Ca_{1-x},Mg_x]CO_3 + CO_2 + H_2O \Leftrightarrow [Ca^{2+}_{1-x} + Mg^{2+}_x] + 2\ HCO_3^-$ *(Eq. 1)*
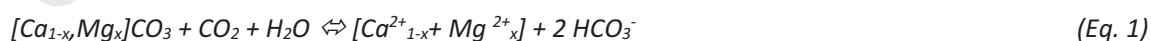
Carbonate dissolution represents 58% of the total DIC (0.36 $Gt.yr^{-1}$) discharged by rivers to the world oceans.

In theory, global warming impacts carbonate dissolution and the chemistry of draining waters in two ways: 1) by decreasing mineral solubility through the temperature dependency of the carbonate dissolution constants (Parkhurst and Appelo, 1999); 2) by increasing the partial pressure of CO_2 (pCO_2) in the soils, epikarsts and caves that determine the initial water characteristics, e.g., water aggressiveness (Peyraube et al., 2012).

According to field observations, CO_2 concentration has risen significantly in Belgian caves since the 1960s (Ek and Godissart, 2014), and the total dissolved solids (TDS) and the alkalinity in river waters have also frequently increased from the 1980s (Raymond et al., 2008; Jeannin et al., 2016). This suggests an increase of pCO_2 driven by various anthropogenic activities (Stets et al., 2014) and/or climate changes.

In soil, the evolution of pCO_2 with an increase in air temperature has not yet been clearly demonstrated. While root respiration increases with global warming (Bond-Lamberty and Thomson, 2010), soil pCO_2 seems to be more controlled by gas diffusion rates (Jones and Mulholland, 1998) and the spatial variability of soil pCO_2 is mainly explained by land cover (Raich and Tufekciogul, 2000). pCO_2 monitoring in soil through time remains too scarce to evidence a relationship with global warming. Previous research on carbonate dissolution investigated an increase in dissolution with air temperature increase (Calmels et al., 2014, Jeannin et al., 2016, Gaillardet et al., 2018) but no quantification of the relationship between air temperature and inorganic carbon flux was clearly established.

At the catchment scale, it is impossible to study the sensitivity of carbonate dissolution to pCO_2 change without taking into account the influence of anthropogenic pollution, which can modify soil acidity. It has already been clearly demonstrated that acid precipitation disturbs silicate bedrock weathering and soil base cation leaching (Probst et al., 1990; 1999). Because strong acid inputs result in a decrease of surface water alkalinity, which is mainly composed of HCO_3^-, stream water acidification is often estimated by the loss of alkalinity (Wright, 1983; Probst et al., 1995). This loss of alkalinity enables the

respective proportions of dissolution due to strong acids such as H_2SO_4 and nitric acid to be calculated (Amiotte-Suchet et al., 1995; Perrin et al., 2008). The acid atmospheric deposition originates from air pollution varying in space and time related to the mix between global and local emission sources of nitrogen and sulfur compounds (Schöpp et al., 2003). The produced strong acids, particularly enhanced under coniferous forests by the capture of dry deposition (Probst et al., 1990; 1995) are leached by rainfall and reach the watersheds. They lead to the acidification of the aquatic ecosystem (Jacks et al., 1984; Probst et al., 1999), springs and groundwater (Jeannin et al., 2016). If the maximum acid deposition was registered during the early eighties in northern countries, the inter-annual trend indicates a regular decrease, observed also in France during the last decades (Pascaud et al., 2016).

Due to the high buffering capacity of carbonate dissolution, the influence of acid precipitation on such lithological conditions has very often been neglected. In karst systems, the predominance of dilution rather than mobilization processes for surface contaminants is driven by karst development, changing from one site to another (Huebsch et al., 2014). Nevertheless, in carbonate areas, the impact of acid anthropogenic inputs, originating either from acid atmospheric deposition or from fertilizer spreading, on carbonate weathering processes has been evidenced by using $\delta^{13}C$ isotopic constraints (Brunet et al., 2011). Indeed, in agricultural areas, strong acid inputs (mainly as nitric acid) originating from fertilizers have been shown to strongly disturbed carbonate weathering processes and associated carbonic acid dissolution by (Perrin et al., 2008).

In remote areas with extensive agriculture, and provided that land use did not change significantly in the last few decades, the local impact of human activities can be considered limited. Thus in such catchments, located far from local anthropogenic sources of strong acids, we hypothesize that the loss of alkalinity -if any- in rivers could come exclusively from two drivers: alkalinity from global warming and alkalinity from acid atmospheric deposition. However, in recent years, the opposing trends of these two drivers (a decrease in acid deposition and an increase in air temperature), should have a similar consequence of increasing alkalinity in rivers draining carbonate rocks.

Selecting catchments far from any local acid pollution, and subjected to different climatic conditions, makes it possible to: (1) link the intensity of carbonate dissolution and the two drivers (air temperature and acid deposition); (2) discuss the long-term trends observed in river chemistry and the CO_2 uptake change induced by a one degree increase in air temperature. Numerous karst systems meet these conditions, because the scarcity of surface water and the thin soil cover in such environments make these catchments inappropriate for intensive agricultural practice on a large scale. Furthermore, the flux of alkalinity is very high in karst areas where carbonate dissolution is highly active (Gombert, 2002). Expressed in terms of surface unit of carbonate outcrop, CO_2 uptake associated with this dissolution process reached 0.71 mol.m^{-2}.year^{-1} in a Chinese karst system (Liu and Zhao, 2000), whereas 0.48 mol.m^{-2}.year^{-1} was estimated for the entire carbonate outcrops at the global scale (Amiotte Suchet et al., 2003).

In this context, we studied the co-evolution of air and water temperatures, river discharge, calcium + magnesium and bicarbonate concentrations in waters for a set of 5 French karst hydrosystems located far from any local source of anthropogenic pollution and monitored weekly over various periods between 1975 and 2006. The aim was to determine the respective impact of air temperature and acid atmospheric deposition on changes in DIC concentration in rivers and consequently, on soil acidity and atmospheric/soil CO_2 uptake by carbonate weathering processes.

2. MATERIALS AND METHODS

2.1 Location of sites, water sampling and analysis

Five well drained karst hydrosystems located in France, where the requisite datasets were available, were selected (Figure 1). They cover a wide range of recharge areas, stream discharges, and average air temperatures (Jourde et al. 2018) (Table 1).

Farfal drains a karst plateau in the Dordogne river basin, under an oceanic climate. This catchment is covered by oak and chestnut forests. Although the average annual precipitation varies between 800

and 1000 mm, evapotranspiration leads to a specific annual discharge ranging from 200 to 350 mm per year.

Fontaine de Vaucluse (FdV) is the only discharge point of a karst hydrosystem which has a much larger recharge area surface (1130 km^2) than the other four sites and is well-known for its considerable mean flow rate of 20 m^{3}s^{-1} (Table 1). More than 98% of the FdV water discharge is supplied by precipitation infiltrated in an area devoid of a perennial hydrological surface network, and mostly covered by a natural Mediterranean vegetation (scrubland). The elevation of 56% of the recharge area ranges between 800 and 1400 m (Fleury et al., 2009).

Lez spring is the main perennial outlet of a Mediterranean karst hydrosystem covered mainly by scrubland, with a groundwater discharge that can reach 15–20 m^3/s during rainfall events and seasonal springs that feed the Lirou river. For the 2008-2015 period, 0.8 m^3.s^{-1} outflowed from the Lez resurgence, 1 m^3.s^{-1} was extracted for drinking water (Charlier et al. 2015) and 0.72 m^3.s^{-1} reached the Lirou river (www.banque.hydro.fr). The Lez spring diffuse recharge area covers 130 km^2. The high average specific discharge (604 L.m^{-2}.yr^{-1}) is due to point recharge draining a hydrogeological basin of about 380 km² (Ladouche et al., 2014).

The Val d'Orléans (ValdO) karst system is the northernmost of the five. It is a hydrosystem covered by alluvia and under the influence of an oceanic climate. More than 80% of the outflowing waters are fed by point recharge from the Loire river, so the impact of local agricultural pollution from the diffuse recharge area on groundwaters is low (Binet et al. 2017). Agricultural inputs to the Loire River are not considered to be a major source of protons in this karst system since protons are already buffered by carbonates located upstream to the ValdO. The major source of protons in this karst comes from the degradation of river organic matter (Albéric and Lepiller 1998). The point recharge strongly increases the average karst discharge per surface area (5631 L.m^{-2}.yr^{-1}). Taking into account weathering reactions and water mixing, the proportion of Ca, Mg, and HCO$_3$ at the spring originating from the losing river

was estimated to be about 70% (Albéric and Lepiller 1998). Thus local karst dissolution contributes to only 30% of the calculated flux.

The Baget karst system, with a land cover dominated by fir-beech forests under a mountainous climate, is located in the Pyrenees Mountains (Southern France). The specific annual discharge is about 1023 $L.m^{-2}.yr^{-1}$. The long time series of the water chemistry dataset for the Baget spring presented here is published for the first time. The spring was sampled weekly for chemical analysis from 1978 to 2005. This is the longest time series ever measured in France for a catchment in a mountain site far from local pollution sources. The pH, total carbonate alkalinity (TCA) and total water hardness were measured using a titrimetric method. The complete chemistry of major ions was analyzed by ionic chromatography during the periods 1982-1996 and 1998-2006. These data (water hardness and TCA for the full period, and Ca^{2+}, Mg^{2+} and alkalinity for part of the period) confirmed that the alkalinity concentration expressed in $mmol.L^{-1}$ was 0.2 TCA and that [Ca+Mg] expressed in $mmol.L^{-1}$ was 0.1 water hardness. Water hardness and TCA were used to determine respectively [Ca+Mg] and [HCO_3] for the full period. Sulfates in open field precipitation were analyzed by ionic chromatography during the periods 1985-1986 and 1994-2006 at the "Balague" station rain gauge located 1km north of the Baget spring.

For the other sites, the available datasets used in this study cover different periods, depending on the site (Table 1). These data are from Bakalowicz (1979), Chery (1983), Marjolet and Salado (1978) and Mudry (1987) for the periods before 1985, and from Albéric and Lepiller (1998), Caetano Bicalho et al. (2012), Emblanch et al. (2003) and Peyraube et al. (2012) for the periods after 1985.

The monthly average air temperature observed for each hydrosystem at the closest climatological station was used to describe the climate trend over the study period: Gourdon for Farfal, Saint Christol for FdV, Saint-Girons for Baget, Montpellier for Lez and Orléans for ValdO. The values of soil or cave pCO_2 were estimated previously by Bakalowicz (1979), Bouzigues et al. (1997), Emblanch (1997) and

Peyraube et al. (2012). Soil pCO_2 was not considered for the Val d'Orléans watershed because waters mainly originate from the Loire River.

Atmospheric deposition data for S and N were extracted for each site from the European interpolation of atmospheric deposits from the EMEP deposition time-series (Schöpp et al., 2003) as performed by Moncoulon et al. (2007). The grid cell is 50x50 km. This model estimates the total annual deposits ($mg.m^{-2}$) of S and N from 1980 to 2010 using the 2006 version of the deposition model. Assuming that H_2SO_4 and HNO_3 are the main source of protons in the atmosphere, the total annual deposition of protons was estimated as the sum of 2S+N (dep_sum ($mol(H^+).m^{-2}.yr^{-1}$)). These deposits were estimated for the grid corresponding to each site.

An order of magnitude of the average water residence time in these karst hydrosystems can be estimated by dividing the volume of the stored groundwaters given by hydrological modelling (particularly rainfall-discharge relationships) by the average karst discharge. The volumes found in the literature for the 5 sites (Binet et al., 2017; Fleury et al., 2009, 2007; Mangin, 1984; Peyraube, 2011) are given in Table 1 and yield estimations of average residence time ranging from 0.14 year (less than 2 months) for Lez to 0.61 year (more than 7 months) for FdV. All the sites have an average water residence time around of less than 1 year. Because of this similar order of magnitude of residence time, the relationship between mean air temperature and average concentration of [Ca+Mg] in karst water averaged for each year can be considered significant. To relate the acid atmospheric deposition data to alkalinity, the annual average concentrations of Ca and Mg in springwaters per decade were used.

2.2. Respective contribution of natural (carbonic acid) and anthropogenic (strong acids) carbonate dissolution to HCO_3 and Ca+Mg streamwater fluxes

During the dissolution of carbonates by carbonic acid (eq. 1), two carbons are produced and released in water as DIC (mainly HCO_3^-). One originates from the carbonate bedrock while the other comes from atmospheric/soil CO_2 as carbonic acid (H_2CO_3) released by the oxidation of soil organic matter (eq.2):

$$CH_2O + O_2 \Leftrightarrow CO_2 + H_2O \Leftrightarrow H_2CO_3^- \Leftrightarrow H^+ + HCO_3^- \qquad (Eq.\ 2)$$

However, the proton from carbonic acid (natural dissolution) can be supplied by strong acids, such as HNO_3 or H_2SO_4. Equation 1 is therefore modified as follows according to the nature of the inputs, nitric acid (eq.3) when considering N-fertilizer inputs (Perrin et al., 2008) or sulfuric acid (eq. 4) when considering acid rain deposition (Amiotte Suchet et al., 1995):

$$[Ca_{1-x}, Mg_x]CO_3 + HNO_3 \Leftrightarrow 1-x\ Ca^{2+} + x\ Mg^{2+} + HCO_3^- + NO_3^- \qquad (Eq.\ 3)$$

$$[Ca_{1-x}, Mg_x]CO_3 + 0,5\ H_2SO_4 \Leftrightarrow 1-x\ Ca^{2+} + x\ Mg^{2+} + HCO_3^- + 0,5\ SO_4^{2-} \qquad (Eq.\ 4)$$
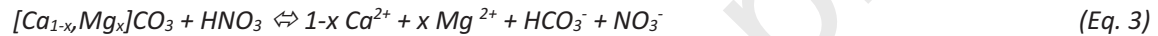
In contrast to equation 1 (natural dissolution) where two bicarbonate ions are released into solution with one [Ca+Mg], anthropogenic dissolution (eq.3 and 4) releases only one bicarbonate ion for one [Ca+Mg].

Consequently, in karst hydrosystems where natural (N) and anthropogenic (A) acids both contribute to carbonate dissolution, the production of [Ca+Mg] in spring waters has two origins. The mass balance can be written as follows:

$$[Ca+Mg]_{total} = [Ca+Mg]_N + [Ca+Mg]_A \qquad (Eq.\ 5)$$

where $[Ca+Mg]_N$ is released by carbonic acid dissolution, $[Ca+Mg]_A$ by strong acid dissolution, and $[Ca+Mg]_{total}$ is the total amount released in spring waters.

With regard to the stoichiometric coefficients, bicarbonate concentration (moles.L^{-1}) can be estimated as follows:

- From equation 1 (natural dissolution with carbonic acid):

$$[HCO_3]_N = 2[Ca+Mg]_N \qquad (Eq.\ 6)$$

9

- From equations 3 and 4 (anthropogenic dissolution with strong acids):

$[HCO_3]_A = [Ca+Mg]_{Al}$ *(Eq. 7)*

For sites subjected to strong acid anthropogenic impacts there is always a mixture of equation 1 and equations 3 and/or 4, which means that the alkalinity ($[HCO_3]_{total}$) measured in spring waters is between 1 and 2 times the total concentration of Ca+Mg ($[Ca+Mg]_{total}$).

Consequently, the loss of alkalinity (Δalk) when going from natural dissolution to a mixture of natural plus anthropogenic dissolution, can be calculated from eq. 5 and 7 as follows:

$\Delta alk = 2[Ca+Mg]_{total} - [HCO_3]_{total} = [Ca+Mg]_A$ *(eq. 8)*

$[Ca+Mg]_N = [Ca+Mg]_{total} + [HCO_3]_{total}$ *(eq. 9)*

2.3.   Impact of air temperature and pCO_2 on carbonate dissolution by carbonic acid

Most of the time, water rock equilibrium between water and calcite is reached in the gaseous-CO_2 production-zone (i.e., the soil) (White 1999). If the CO_2 loss through dissolution is permanently replenished by root respiration, organic matter mineralization and exchange with the CO_2 in the infiltration zone (eq. 2), the partial pressure of CO_2 (pCO_2) remains constant. In these conditions, [Ca+Mg] production is limited by the saturation of water with carbonate (Calmels et al., 2014). To test this hypothesis, the saturation indexes of karst waters were estimated for calcite (ISc) and for dolomite (ISd), the two extreme end-members of the carbonate solid solution using the PhreeqC model (Appelo, 1994).

Assuming that: (i) the chemical reactions (cf. Eq. 1, 3 and 4) occurred in an open system with the phases being in equilibrium with calcite; (ii) the pCO_2 ranged from $10^{-1.5}$ to $10^{-2.5}$ atm, and (iii) as a basic hypothesis, carbonates are dominated by calcite (White, 1999, Calmels et al., 2014), the concentration in [Ca+Mg] released in springwaters by carbonic acid dissolution can be estimated following the equation below (Drever, 1997):

$$[Ca+Mg]_N = \left(\frac{K_1 K_H K_{SP}}{4 K_2 \gamma_2 \gamma_1^2} * pCO_2\right)^{1/3}$$ *(Eq. 10)*

where γ_1 and γ_2 are the activity coefficients for Ca^{2+} and HCO_3^- ions, respectively; K_1 and K_2 are the first and second dissolution constants of carbonic acid, respectively; K_{sp} is the solubility product of calcite and K_H, the Henry's constant of CO_2.

Because the thermodynamic constant evolves with the temperature, an air temperature *vs.* $[Ca+Mg]_N$ scattergram can be drawn with theoretical curves representing $[Ca, Mg]_N = f(T_{air}, pCO_2)$ in order to compare theoretical data with field measurements.

2.4. Flux calculation, regression analysis and uncertainties

HCO_3^-, Ca and Mg concentrations present a chemostatic behavior in rivers, *i.e.* concentration is independent of hydrological changes. For these kinds of dissolved elements, the correlation between concentration (C) and discharge (Q) is weak (Godsey et al., 2009). For these reasons, a simple flux calculation method was used to estimate the annual fluxes (F):

$$F = K.\bar{Q}.\sum_{i=1}^{n}(C_i/n) \hspace{4cm} \textit{(eq. 11)}$$

where F, the annual flux (mol.m^{-2}.yr^{-1}), is the product between $\bar{Q}$, the annual average discharge, Ci the observed concentrations and n the number of samplings (i) for concentration measurements in a year. K is a constant in order to respect unit changes. The F flux will be used to perform the mass balance between input and output.

In the flux calculation, the range of discharge variations is two orders of magnitude higher than the range of concentration changes. Thus the main driver of flux changes is the discharge and the concentration changes are difficult to evidence by taking only the flux values into account. By calculating flux at average discharge, the concentration changes in the studied flux can be captured (Raymond et al., 2008). In our case $\bar{Q}$ in equation 10 becomes the average inter-annual discharge given in table 1.

The inter-annual and the spatial variability of fluxes were compared to the annual flux at average discharge and to the annual average temperature using a linear regression (y=ax+b). The regression is based on a Pearson test given a slope (a) and an ordinate of origin (b).The quality of the regression was

estimated using the Pearson coefficient r^2 and a p value < 0.001. The better of the two descriptors (i.e., air or spring temperature) was selected by comparing r^2 coefficients for the two regressions. To test the robustness of the coefficient, six regressions were computed using the overall dataset (5 sites) and then using only 4 sites, excluding the sites one after the other (Table 4 and 5). The average value and standard deviation of a, b and r were calculated from these 6 tests. To test the sensitivity of the slope between temperature and the natural flux of Ca+Mg graphically, x and y error bars were added to this graph. Error bars include (1) statistical errors (2) errors linked to the choice of descriptor (the range between air and spring temperature will enable the X bar to be drawn) and (3) errors linked to Ca, Mg and HCO_3 origin. If x $mmol.L^{-1}$ of Ca or Mg has another origin than the carbonates, then equation 9 says that the natural concentration is an overestimation of x and equation 8 says anthropogenic concentration will be overestimated by about 2 times. The maximum value of x is estimated in the Discussion section, enabling positive Y bars to be drawn on the $[Ca+Mg]_N$ =f(temp) plot. The only way to under-estimate the natural flux is to introduce an error on HCO_3. The negative Y bars assume an analytical uncertainty of about 5% on HCO_3.

The respective impact of air temperature and of acid atmospheric deposits on [Ca+Mg] and [HCO_3] in stream waters can be estimated from the linear regressions proposed above. Applied to the Baget site, where the time series is the longest, theoretical $[Ca+Mg]^*_A$ and $[Ca+Mg]^*_N$ were calculated using the regression coefficients of the linear relationships, respectively with air temperature, average discharge and total atmospheric acid deposits. The temporal evolutions of these modeled values were compared with the observed ones.

3. RESULTS

3.1. Water chemistry characteristics of the studied karst hydrosystems and atmospheric deposits

The Baget site has the most complete time series for [Ca+Mg], [HCO_3] and daily discharge. Figure 2 illustrates the high variability [0.04-7.21] of discharge ($m^3.s^{-1}$) compared to the variability in [Ca+Mg] and [HCO_3] concentrations, respectively [2.43-3.74] and [2.72-4.19]. The temporal variability of

discharge, [Ca+Mg], and [HCO$_3$] is mainly seasonal with peaks during high water flow. A long term component is also visible for [Ca+Mg] and [HCO$_3$] concentrations. In 1990 a long term pumping test dried the Baget spring, so no data were available for this year.

In Table 2, the average and standard deviation of the different parameters observed are summarized for each site, for the whole periods studied. Table 3 presents the concentrations and fluxes of the different elements in each year. Average air temperature ranged between 9.0 °C at the FdV recharge area in 1981 and 17.7°C for the Lez system in 2003. Considering the annual average, all the pH values are above 7. The [Ca+Mg] concentration covers a large range, from 1.11 mmol.L^{-1} at the ValdO site (1994) to 3.49 mmol.L^{-1} at the Lez site (2007), whereas [HCO$_3$] concentration ranges between 1.84 mmol.L^{-1} at the ValdO site (1980) and 6.08 mmol.L^{-1} at the Lez site (2007).

In these waters, applying equations 5 and 8, the calculated proportion of [Ca+Mg] released from the dissolution of carbonate due to atmospheric acid deposition ([Ca+Mg]$_A$) was about 13 to 41% of the total [Ca+Mg] concentrations (Table 3). All the waters are over-saturated regarding calcite (lsc), and are under-saturated or saturated regarding dolomite (lsd). Finally, after a significant increase until the 1980s like other places in the northern hemisphere (Schöpp et al., 2003), acid atmospheric deposition was halved from 1980 to 2005, decreasing at the Baget site from 0.23 to 0.10 mol.m^{-2}.yr (Table 3), consistently with other sites in France located in remote areas (Pascaud et al., 2016).

3.2. Relationship between [Ca+Mg] and [HCO$_3$] concentrations in spring waters

Monthly values of [Ca+Mg] *vs.* [HCO$_3$] concentrations in spring waters are plotted on Figure 3. All concentrations are located between the 1:2 and 1:1 lines, which represent the stoichiometric ratio Ca+Mg/HCO$_3$ of equations 1 and 3 or 4, respectively. For all the data from the 5 sites, more or less substantial discrepancies occur between observed values and the 1:2 theoretical line of natural dissolution with carbonic acid. For each site, the cluster of points is well lumped, except for the FdV site, where the waters sampled in 2006 tend towards the 1:1 line (identified in Figure 3 and 4).

3.3. Relationship between [Ca + Mg]$_A$ and Mg concentration

The amount of [Ca+Mg] released by strong acid carbonate dissolution, or so-called [Ca+Mg]$_A$ is in the same order of magnitude as the Mg concentration (Figure 4). The ValdO, Farfal and Lez sites show an increase in [Ca+Mg]$_A$ linked with an increase in Mg concentration. The Baget spring waters present higher concentrations in Mg, but the relation between [Ca+Mg]$_A$ and Mg is also positive and significant. The FdV waters show the greatest dispersion and a relatively constant Mg concentration for increasing [Ca+Mg]$_A$ particularly for the period 2006-2007, although the data before 2005 follow the same pattern as at the other sites. This relationship illustrates the role of Magnesium in [Ca+Mg]$_A$ variability.

3.4. Relationship between [Ca+Mg]$_N$ and air temperature

The [Ca+Mg]$_N$ in spring waters *vs*. air temperature presented for each karst system (Fig. 5) illustrates the [Ca+Mg]$_N$ variability. The continuous decreasing lines represent the theoretical evolutions of [Ca+Mg]$_N$ with air temperature for different pCO$_2$ values in atm ($10^{-2.6}$ $10^{-2.2}$, $10^{-1.8}$, $10^{-1.4}$). The [Ca+Mg]$_N$ observed for the Baget hydrosystem presents a variability that is well described by the theoretical relationship corresponding to a pCO$_2$ value of $10^{-2.6}$ atm. This calculated value is close to the winter soil pCO$_2$ observed by Bakalowicz in 1979 (Table 1). The FdV dataset is located between the pCO$_2$ lines of $10^{-2.6}$ and $10^{-1.8}$ atm, whereas those of the Lez and Farfal sites are in equilibrium with higher pCO$_2$ values ($10^{-1.8}$ to $10^{-1.5}$ atm.) In the same way, for these 3 sites, the soil pCO$_2$ values observed during summer and winter (Table 1) fall within the bounds of the theoretical pCO$_2$ needed to explain the [Ca+Mg]$_N$ variability (equation 10). The ValdO site data lie below the $10^{-2.6}$ line. [Ca+Mg]$_N$ increases with air temperature in ValdO, Baget and to a lesser extent at the Lez site.

3.5. Relationship between [Ca + Mg]$_A$ flux and atmospheric acid deposition

At the yearly scale, the specific flux of [Ca + Mg]$_A$ in spring waters released from carbonate dissolution by the protons originating from strong acid atmospheric deposition was compared with the specific flux of 2S+N deposited to the corresponding hydrosystem by atmospheric deposition (Figure 6). This flux is considered to be close to the proton flux (Dep_sum). Most of the points are above the line 1:1. The highest values of atmospheric deposits of 2S+N observed in 1975, 1979, 1985 are consistent with

high values of the anthropogenic fraction of the [Ca+Mg] flux F (F[Ca+Mg]_A). The linear regression (dotted line in Figure 6) has a slope of 1.05+- 0.31 (Table 4), but with a non-zero intercept. Whatever the sites chosen for the regression, the Pearson correlation coefficients are significant for a probability (p value) below or equal to 0.001. FdV 2006 shows a strong flux of $[Ca+Mg]_A$ with respect to atmospheric deposition.

3.6. Relationship between $[Ca+Mg]_N$ flux and air temperature

The correlation between water temperature and $F[Ca+Mg]_N$ (a=0.064; b=0.62 r^2= 0.50, n=34) is less significant than the correlation with air temperature (a=0.059; b=0.60 r^2= 0.73, n=51) leading to select air temperature as the main descriptive variable in this paper. Figure 7 presents the relationship between $[Ca+Mg]_N$ flux and air temperature for several years. Taking each site individually, it is difficult to find a significant correlation between flux and air temperature, but considering all the sites together, one can observed a positive relationship between $[Ca+Mg]_N$ flux and air temperature. Farfal and the year FdV 2006 are the outliers of this relationship.

The description of the parameters of this relationship is given in Table 5. Whatever the combination of sites considered, the regression coefficients are above 0.41 with a significant p values. The average slope of the relationship between $[Ca+Mg]_N$ flux and air temperature is 0.061 $mol.m^{-2}.yr^{-1}.°C^{-1}$ with a standard deviation of 0.006 $mol.m^{-2}.yr^{-1}.°C^{-1}$. The uncertainty about the most appropriate temperature to describe the reaction, i.e. air or spring temperature, can be represented with an error range covering the range from air to spring observations (X in Figure 7). Uncertainties on calcium origin, calcite precipitation, and initial river input were quantified with Y error bars. Values are discussed in the next chapter.

3.8. Seasonal and inter-seasonal fluctuations of the concentrations

Annual acid deposition, and monthly evolutions of sulfates in open field precipitation, air temperature, $[Ca+Mg]$, $[HCO_3]$ and $[Ca+Mg]_A$ and $[Ca+Mg]_N$ are presented in Figure 8 for the Baget site. The air temperature is maximum in August-September, around 16°C, and minimum in December and January with 5°C. The spring discharge is maximum in January to March and minimum in September-October. The $[Ca+Mg]_A$ fluctuations are the opposite of the discharge variations, with a maximum (0.7 mmol.L^{-1}) in September-October and a minimum (about 0.3 mmol.L^{-1}) between January to March. In contrast, $[Ca+Mg]_N$ is maximum (1.4 mmol.L^{-1}) in December-January and minimum (about 1 mmol.L^{-1}) in August-September, in inverse variation to air temperature.

Figures 8 A, B and C give the temporal fluctuations of sulfates in open field precipitation, the water discharge and air temperature over the period 1979-2009 for the Baget hydrosystem. The decomposition of $[Ca+Mg]_{total}$ into $[Ca+Mg]_A$ and $[Ca+Mg]_N$ exhibits opposite trends over the period recorded (see yearly average trends in Figures 8D, E). $[Ca+Mg]_A$ increased during the 1980s and then decreased for the rest of the period, while at the same time $[Ca+Mg]_N$ increased from 1989.

These long-term trends in yearly average can be compared with the long-term evolution of $[Ca+Mg]^*_A$ and $[Ca+Mg]^*_N$ (equation 12 and 13) derived from linear regressions using air-temperature and atmospheric deposits and average discharge as input data and presented above in tables 4 and 5.

$[Ca+Mg]_A{}^* = (1.05{*}dep\_sum + 0.31) / Sp. \ Discharge$ \hspace{2em} (eq.12)

$[Ca+Mg]_N{}^* = (0.061{*}Tair + 0.59) / Sp. \ Discharge$ \hspace{2em} (eq. 13)

These concentrations can be calculated for the years where the atmospheric deposits of protons and average air temperature are available. These long-term trends of the yearly average concentrations are represented by black lines on Figure 8D and 8E. $[Ca+Mg]^*_A$ reached a maximum value in 1985 while $[Ca+Mg]^*_N$ increased slowly from 1979. These differences are used in the following section to discuss the respective impacts of global warming and atmospheric acid deposition on the long term evolution of $[Ca+Mg]_{total}$ concentrations.

4. DISCUSSION

4.1. Origin of calcium, magnesium and bicarbonate in karst waters and ensuing uncertainties

The concentrations of calcium, magnesium and bicarbonates are in the range of variability observed in Europe (Perrin et al, 2003; Binet et al., 2006; Mudarra and Andreo, 2010). The distribution of [Ca+Mg] *vs* [HCO_3] concentrations (Figure 3) between the stoichiometric lines 1:1 (anthropogenic dissolution) and 1:2 (natural dissolution) shows that the two dissolution processes, by carbonic and strong acids, respectively take place on the 5 sites. The proximity with the 1:2 line confirms that the catchments are in remote areas or undergo very low agricultural pressure. From the location of the points between the two theoretical lines the respective parts of strong acids and carbonic acid in the control of carbonate dissolution can be estimated. The proximity of the points with the 1:2 line shows that carbonic acid dissolution is predominant.

The seasonal evolution of SO_4 in rain shows the same dynamic as $[Ca+Mg]_A$, with an annual peak that is delayed compared to discharge, air temperature and $[Ca+Mg]_N$ peaks. The co-evolution of $[Ca+Mg]_A$ and magnesium (Figure 4) suggests that they have the same behavior. Even if a small proportion of Ca and Mg in karst waters may originate from continental dust (Pascaud et al., 2016), the hypothesis that the entire Mg flux in karst hydrosystems originates from the atmosphere, supplied by atmospheric precipitation, is not sustainable. This hypothesis is in contradiction with several previous studies (Batiot et al., 2003; Binet et al., 2006; Emblanch et al., 2003) and is also inconsistent with rock mineralogical analysis, showing that carbonates contain magnesium (Monnin et al., 1998).

The most probable explanation is that carbonates are not a solid solution, but a patchwork of calcite and dolomite. In soil, the weak carbonic acid dissolves the most soluble mineral i.e. the calcite since the dissolution constant of dolomite is lower than that of calcite. Protons from strong acids such as sulfuric and nitric acids mainly supplied by rainwater are more efficient at dissolving carbonate minerals with a lower solubility, such as dolomite or magnesian calcite. Beaulieu et al. (2012) suggested such a mechanism in the Mackenzie River Basin, with a chemical weathering of the dolomite minerals increasing while the annual calcium flux from calcite dissolution remained almost unchanged. The

17

saturation of water with regard to calcite (Table 3), but its undersaturation to dolomite, sustains this hypothesis. From the monitoring of 55 springs in France, Peyraube et al. (2019) observed that HCO_3 increases with 2*Ca, following the theory of carbonic dissolution. The fact that this relationship does not take Mg into account validates the present discussion. Figure 4 suggests that the average values of magnesium from one site to another are controlled by a strong acid inputs on the sites (first order), but that the Mg dispersion for a single site seems to be related with a strong dispersion in the water residence time (second order).

Lastly, some changes in the [Ca+Mg] concentrations could be explained by a changing ratio of the mixing between transmissive and capacitive zones as demonstrated by Charmoille et al. (2009). This could explain the observed variability between sites, or during exceptional years (see FdV 2006). Changing the residence time can favor dolomite dissolution. In this hypothesis, 2 HCO_3 will be produced for 1 Mg and the concentrations will increase along a 1:2 slope. This can also favor calcite deposition, consuming 1 Ca for 1 HCO_3 affecting [Ca+Mg].

All these hypotheses have been tested in terms of uncertainty on $[Ca+Mg]_N$. Following equation 8 and 9, calcite precipitation, which consumes 1 Ca for 1 HCO_3, leads to an overestimation of $[Ca+Mg]_A$, but has not influence on $[Ca+Mg]_N$. Whatever the hypothesis, the uncertainties on Ca origin never underestimated $[Ca+Mg]_N$, which can be considered as a minimum value. Only the uncertainty on HCO_3 can underestimate $[Ca+Mg]_N$. In these carbonate areas, the uncertainty on HCO_3 come from the uncertainty on the initial river composition, difficult to evaluate.

4.2. Anthropogenic influence on the carbonate dissolution process

4.2.1. Role of acid atmospheric inputs

The average values of observed $[Ca+Mg]_A$, 0.29 to 0.79 $mmol.L^{-1}$ (Table 2), are close to the alkalinity loss values given for a forested area in Perrin et al. (2008) and much lower than the values found in rivers draining agricultural catchments, values that can reach 5 $mmol.L^{-1}$. The flux of $[Ca+Mg]_A$ is well correlated with atmospheric acid deposition (Figure 6 and Table 5) and has decreased since 1975. This pattern, based on sites that are several hundreds of kilometers apart, confirms that the main driver is

of atmospheric origin. The slope of the relationships calculated from the regressions involving the different sites is close to 1. This suggests that changes over time in the inputs of strong acid by atmospheric deposition are balanced by changes in carbonate dissolution and in karst water outputs of $[Ca+Mg]_A$. Because the average residence time of water is less than one year (Table 1), the fluxes of H^+ from anthropogenic origin are neutralized by an excess of carbonate dissolution, which releases an excess of [Ca+Mg] to spring waters.

The average intercept of the regressions related to $[Ca+Mg]_A$ (0.31 ±0.03 mol.m^{-2}.yr^{-1} given in table 5) represents the proportion of Ca+Mg flux that is not explained by atmospheric deposition or by temperature and is considered as the proportion of Ca+Mg whose origin is questionable.

The origin could be explained by another strong acid source of geological origin such as sulfuric acid from pyrite oxidation (Binet et al., 2009) or nitric acid from fertilizers for some of the sites (Perrin et al., 2008). For the former case, this strong acid might be present and the flux appears to be constant from the 1980s except for the FdV 2006 outliers. N runoff from fertilizer is a potentially large confounding variable. However, the study areas were selected so as to be far from intensive agriculture and the maximum values of spring NO_3 concentrations found in the literature are 0.17 (Baget), 0.15 (FdV), 0.43 (VdO), 0.21 (Farfal), 0.15 (Lez) mmol.L^{-1}, confirming that fertilizers are not a main issue with respect to $[Ca+Mg]_A$ variability, which ranges monthly from 0.1 to 1.84 mmol.l-1. A second explanation is that atmospheric deposits are generally underestimated by about 0.31 mol.m^{-2}.yr^{-1} since dry deposition truly captured by vegetation (particularly coniferous cover, Probst et al., 1995) is not taken into account in open field measurements or modelled EMEP data. Moreover, the uncertainties of EMEP modelled data from grid to site should also be mentioned, as pointed out by Schöpp et al. (2003). The protons captured by cation exchange in soils (Probst et al., 1990) might be a third explanation for the higher Ca+Mg flux with regard to proton flux deposition. Calcium may be released during the replacement of calcium by protons or ammonium. As observed by Bobbink et al. (1992), the amount of cations (among which Ca and Mg) lost from the canopy was in good agreement with the observed

ammonium uptake by the same canopy. Indeed, the opposition between discharge and $[Ca+Mg]_A$ observed at the Baget site (Figure 8F) suggests that acid pollution is diluted during winter atmospheric precipitations. Probst et al. (1990) showed that even in remote places, the atmosphere may be more polluted in winter, but that the spring waters are less impacted due to dilution processes from large aquifer storage.

Finally, if the average 0.155 mol.m^{-2}.yr^{-1} of Ca has another origin than carbonate dissolution, this would explain the 0.31 mol.m^{-2}.yr^{-1} overestimation observed in the anthropogenic flux (equation 8), and these 0.155 mol.m^{-2}.yr^{-1} have to be considered as a positive uncertainty in the $[Ca+Mg]_N$ flux estimation to take into account all the possibilities mentioned in this section.

4.2.2 Role of air temperature increase

Air temperature and pCO_2 seasonal fluctuations explain the main variability of the observed $[Ca+Mg]_N$ (Figure 5), with a solubility increase in cold water in a saturated system with regard to calcite. If a 0.2 saturation index uncertainty is accepted, all the waters are calcite-saturated (Table 3). The decreasing solubility with air temperature increase explains the seasonal evolution of the Baget spring water concentrations in $[Ca+Mg]_N$ with higher concentrations in winter. Baget pCO_2 seems to be stable over the years, with an average value close to $10^{-2.6}$ atm as observed in soil during winter (Table 1). For FdV, Lez and ValdO, the dispersion of $[Ca+Mg]_N$ seems mainly driven by pCO_2 change rather than by carbonate solubility (Figure 5). For Farfal, the $[Ca+Mg]_N$ is relatively constant. Peyraube et al. (2013) established that CO_2 in this massif varies little with the season, as it is driven by a water temperature that is closer to the annual average temperature of air, as found here in figure 5. At the yearly scale this uncertainty on the temperature descriptor (air or water) is not significant, except for FdV with contrasted elevations between the spring and the infiltration area, The good match between soil pCO_2 estimated for each site with Figure 5 and soil pCO_2 measured in the field (Table 1) suggests that the assumption of an open system is acceptable.

Based on the discussion of the origin of magnesium, associated with $[Ca+Mg]_A$, it follows that $[Ca+Mg]_N$ is more associated with a calcite endmember contribution. In this case, the dissolution equation

constants for the calcite appear to be suitable. If total [Ca+Mg] were used to examine the relationship between pCO_2 and air temperature, a discrepancy would be observed between [Ca] concentration and pCO_2, as observed in Calmels et al. (2014). Moreover, the data suggest a seasonal evolution of pCO_2 between winter and summer. This would lead to a distorted interpretation, because these seasonal changes in Ca+Mg are driven by dilution of [Ca+Mg]$_A$ during high flows in winter and not by the change in air temperature.

The correlation between average discharge flux of [Ca+Mg]$_N$ and air temperature is significant. If each site is considered separately, the relationship between air temperature and [Ca+Mg]$_N$ flux is not obvious. But considering all the sites together, the correlation becomes significant (p-value <0.001) despite the Farfal and 2006 FdV outliers (Figure 7). The Farfal case may be due to the limits of the system, that cannot be clearly defined, and to the shorter period of observation (2 years) than at the other sites. This may be the cause of uncertainty on the average discharge estimation. Concerning the FdV 2006 case, pollution by a strong acid or calcium from another origin than carbonate(such as marine transport and industrial emissions sources and dusts from Sahara observed in this region, (Pascaud et al., 2016) as already mentioned, may have interfered in the calculation of natural [Ca+Mg].

With regard to the average slope of the regressions in Table 5 (0.061 $\pm$0.006 mol.m^{-2} y^{-1} °C^{-1}), and according to an average specific discharge of 300 L.m^{-2}.yr^{-1} (corresponding to the French average runoff given by Abbaspour et al., 2015), the total [Ca+Mg] concentration should increase per degree of 204 µmol.L^{-1}.°C^{-1}. This estimation can be compared with the [Ca+Mg] concentration gradient observed in the Jura Mountains with increasing air temperature. Along a temperature gradient in the Jura Mountains, Calmels et al. (2014) estimated that 35% of the [Ca] increase from 1600 µmol.L^{-1} to 3000 µmol.L^{-1}, i.e. 490 µmol.L^{-1}, was caused by a 4.5°C air temperature gradient, given an increase per degree of about 108 µmol.L^{-1}°C^{-1}. In these mountains, a time series analysis suggested a +2.13 µmol.L^{-1}.yr^{-1} increase of Ca and no significant change in Mg in parallel to a 0.022°C.yr^{-1} air temperature increase (Jeannin et al., 2016). Without subtracting the impact of atmospheric acid deposition, these values

lead to 97 µmol.L^{-1}.°C^1 of Ca+Mg, which is logically slightly lower than our estimation. In these studies, the rough estimation of atmospheric acid deposits leads to an underestimation of the [Ca+Mg]$_N$ flux change with air temperature. From error bars, extreme slopes including uncertainties on the origin of elements (grey dotted lines) can be proposed and values range between 0.010 to 0.095 mol.m^{-2}. °C^{-1}. The choice of a linear relationship seems appropriated when air temperature vary between 5°C to 20°C. The relationship appears to be more complex at the global scale where air temperature vary between -15°C to 30°C (Gaillardet *et al.* 2018).

The fact that [Ca+Mg]$_N$ flux is correlated with air temperature at constant discharge means that: (1) for a given site, there is on average an equilibrium between CO_2 production in soil and dilution by recharge; (2) the possible loss/gain of discharge linked with a 1°C air temperature increase is not taken into account in this correlation. Because the annual fluxes of [Ca+Mg]$_N$ and the [Ca+Mg]$_A$ are not correlated with air temperature, it seems that during a year, pCO_2 is not influenced by the dilution caused by rainwater. The hydrological effect of rainfall on carbonate dissolution and pCO_2 is indirect. The increase in air PCO_2 is too low to explain this flux evolution. One explanation could be that after several years of dryness, the vegetation adapts its biomass production, influencing the pCO_2 in soil by a lower mineralization of organic matter (Bloor and Bardgett, 2012). In the same way, this positive correlation at the yearly scale could be due to an increase in subsurface pCO_2 with increasing surface temperature, either *via* increased microbial activity and root respiration, or due to change in the density-driven ventilation of the epikarst during colder periods (James et al. 2014). Following Quinif et al. (2014) and Dubois et al. (2014), bacteria may be at the base of the dissolution processes, which may partly explain the observed link between higher pCO_2 (due to a higher temperature that activates the bacteria activity) and higher solubility of carbonate. This causes a long term sliding of the seasonal temperature / [Ca+Mg]$_N$ relationship. In stalagmites, <delta>^{13}C evidences that the long-term T-PCO_2 link is directly influenced by the vegetation and bacterial activity in the soil, related with soil PCO_2. This relation was proved to follow Dansgaerd-Oeschger changes in the last Glacial Period (Genty et al. 2003). This is an argument for a strong relationship at a longer term between pCO_2 and air T.

4.2.3. Consequences on the trends observed in concentration time series.

The correlation coefficients (tables 4 and 5) were used to describe the time series evolution of the concentrations observed at the Baget site from air temperature, acid deposits, average discharge and annual average discharge (Figure 8). Concerning $[Ca+Mg]_A$, the interannual trend observed in Baget and the $[Ca+Mg]_A$* values estimated from the linear regression analysis (Table 5) follow the same trend, increasing until the 1980s and then decreasing slowly. Concerning $[Ca+Mg]_N$, even if in the correlation with air temperature (Figure 7, Table 4) the distribution of the Baget samples is very lumped, the regression coefficients calculated for the time fluctuation of $[Ca+Mg]_N$ (dotted line, Figure 8), show the same trend as the annual average values observed, slowly increasing from 1985 on. Atmospheric deposition, air temperature and average discharge are therefore three descriptors that can describe the long term trends in water chemistry.

4.3. Consequences on the fluxes during the last decades

4.3.1. On base cation fluxes

The total Ca+Mg fluxes estimated for each site (Table 3) and averaged yearly (Table 2) are in the range of those commonly estimated for Europe 0.13 – 2 mole.m^{-2}.year^{-1} of Ca+Mg fluxes (Bakalowicz, 1979).

The [Ca+Mg] fluxes induced by atmospheric acid deposits, F[Ca+Mg]$_A$ are in the same order of magnitude for the 5 sites studied here. Following the stoichiometry of equations 3 and 4, F[Ca+Mg]$_A$ must be equal to the inputs of protons. The data obtained here are higher than the total atmospheric inputs of protons estimated at 0.18 mol.m^{-2}.year^{-1} flux observed in a granitic area of the Vosges Mountains (Probst et al., 1992) , 0.11 at the Aubure watershed and 0.044 in Mont Lozère in South Central Massif (Probst et al., 1995). This can be explained in two ways: (1) a strong acid is missing to explain the whole variability of $[Ca+Mg]_A$ at these site, or (2) $[Ca+Mg]_A$ may be overestimated, because part of the Ca in solution does not originate from carbonate dissolution.

4.3.2. On CO_2 fluxes

The stoichiometric coefficients of equation 1 show that CO_2 flux uptake in soil/atmosphere is equal to F_$[Ca+Mg]_N$. Compared to the CO_2 flux consumed by carbonate dissolution in different regions in the world, (0.48 mol m^{-2} yr^{-1} at a global scale, Amiotte Suchet et al., 2003; 0.71 mol m^{-2} yr^{-1} for Chinese

karst hydrosystems, Liu and Zhao, 2000; 0.5 mol m^{-2} yr^{-1} for the Alpine river basins, Liu and Zhao, 2000; Amiotte Suchet et al., 2003; Donnini et al., 2016; Liu and Zhao, 2000), the CO_2 flux values estimated in France (from 0.80 to 1.49 mol m^{-2} yr^{-1}) are in the same order of magnitude but slightly higher, particularly for the sites with a high water specific discharge (Table 1). The karst systems where allogenic flows into swallow holes are the main recharge present higher specific CO_2 fluxes. The chemical reactions are exacerbated when surface waters reach the carbonates. As expected, the variability of CO_2 fluxes from one hydrosystem to another is driven by the variability of the water recharge (White, 1999). Consequently, the more fully developed the karst conduit network is, the more the hydrosystem is a CO_2 consumer for carbonate dissolution. Our results suggest that well-developed karst hydrosystems are hot-spots for CO_2 uptake.

According to Equation 1, the CO_2 flux is equal to $F\_[Ca+Mg]_N$, so CO_2 flux is also temperature dependent, with a slope of 0.061 ±0.006 mol.m^{-2} y^{-1} °C^{-1}. As shown above, the CO_2 uptake can be estimated by fixing an average specific discharge at 300 L.m^{-2}.yr^{-1}. According to this hypothesis, the global warming CO_2 uptake *versus* air temperature increase would be about +204 µmol.L^{-1} °C^{-1}.

For the Baget site, a 1°C increase in air temperature would increase the CO_2 uptake by about 5.7% of the CO_2 average flux. As already mentioned, there are several, sometimes opposing, causes for this relationship such as a change in soil pCO_2, but also changes in evapotranspiration or in the amount of rainfall. In mountainous regions, a temperature increase creates an early snow melting (Szczypta et al., 2015), changing the seasonal flood distribution. This change can also affect the CO_2 fluxes consumed by carbonate dissolution, especially in March–April when increasing fluxes of $[Ca+Mg]_N$ are released in karst waters.

4.3.3. On initial soil /epikarst pCO_2

Following the slope of the proposed regression (Table 4) and fixing the average discharge at about 1023 L.m^{-2}.yr^{-1} (an example of a high value in table 1: Baget), the increase in $[Ca+Mg]_N$ for a 1°C increase in air temperature should be about +58 µmol.L^{-1}.°C^{-1}. However, if we use a discharge corresponding to the average hydroclimatic conditions of the sites (about 300 L.m^{-2}.yr^{-1}), the increase in $[Ca+Mg]_N$ will

be about +204 µmol.L^{-1}.°C^{-1}. Since the input pCO$_2$ is not linked with the water flux but with the [Ca+Mg]$_N$ concentrations in waters (eq. 10), this suggests that the pCO$_2$ increase with air temperature will be stronger in low rainfall areas. A concentration effect, due to the slower leaching of soil, can explain this phenomenon.

5. CONCLUSION

The decomposition of [Ca+Mg] into [Ca+Mg] from strong acids and that from carbonic acid evidences that the temporal changes in carbonate dissolution are driven by surface boundary conditions, i.e. atmospheric acid pollution, surface pollution in the catchment and increase in air temperature.

By estimating the amount of carbonate dissociated by strong acids, using measurements in calcium, magnesium and bicarbonate concentrations, the impact of acid atmospheric deposition on surface waters from the 1970s can be reconstructed, reinterpreting the water chemistry of karst waters in this new framework.

The correlation between atmospheric acid deposition and karst waters has evidenced that these waters are highly sensitive to surface processes. The dephasing caused by seasonal fluctuations between proton input and [Ca+Mg] output is due to the water residence time in these systems. An output could be a new tracer of the water residence time for the range 1 to 12 months.

The estimation of the amount of carbonate dissociated by carbonic acid and the associated CO$_2$ uptake changes over the seasons, linked to the mineral solubility that increases concentrations in winter, and evolves over the decade because of pCO$_2$ change. As CO$_2$ uptake was found to be partially hidden by acid atmospheric pollution, the estimation of CO$_2$ uptake fluxes in the literature may be underestimated. Even if the proposed estimation is rough, this is one of the first times that a value of the CO$_2$ uptake change under global warming is proposed, based on field observations of the critical zone. Concerning this negative feedback with atmospheric carbon, the recharge is the main variable driving the CO$_2$ uptake fluxes, suggesting that well-developed karst systems with a high recharge rate are hot-spots for atmospheric CO$_2$ uptake.

ACKNOWLEDGMENT

REFERENCES

1. Abbaspour, K.C., Rouholahnejad, E., Vaghefi, S., Srinivasan, R., Yang, H., Kløve, B., 2015. A continental-scale hydrology and water quality model for Europe: Calibration and uncertainty of a high-resolution large-scale SWAT model. J. Hydrol. 524, 733–752. https://doi.org/10.1016/j.jhydrol.2015.03.027

2. Albéric, P., Lepiller, M., 1998. Oxydation de la matière organique dans un système hydrologique karstique alimenté par des pertes fluviales (Loiret, France) / Oxidation of organic matter in a karstic hydrologic unit supplied through stream sinks (Loiret, France). Water Res. 32, 2051–2064. https://doi.org/10.1016/S0043-1354(97)00439-9

3. Amiotte Suchet, P., Probst, A., Probst, J.L., 1995. Influence of acid rain on CO2 consumption by rock weathering: Local and global scales. Water. Air. Soil Pollut. 85, 1563–1568. https://doi.org/10.1007/BF00477203

4. Amiotte Suchet, P., Probst, J.-L., Ludwig, W., 2003. Worldwide distribution of continental rock lithology: Implications for the atmospheric/soil CO2 uptake by continental weathering and alkalinity river transport to the oceans. Glob. Biogeochem. Cycles 17, n/a-n/a. https://doi.org/10.1029/2002GB001891

5. Appelo, C.A.J., 1994. Cation and proton exchange, pH variations, and carbonate reactions in a freshening aquifer. Water Resour. Res. 30, 2793–2805. https://doi.org/10.1029/94WR01048

6. Bakalowicz, M., 1979. Contribution de la géochimie des eaux à la connaissance de l'aquifère karstique et de la karstification. Universite Pierre et Marie Curie, Paris.

7. Batiot, C., Emblanch, C., Blavoux, B., 2003. Carbone organique total (COT) et magnésium (Mg2+) : deux traceurs complémentaires du temps de séjour dans l'aquifère karstique. Comptes Rendus Geosci. 335, 205–214. https://doi.org/10.1016/S1631-0713(03)00027-0

8. Beaulieu, E., Godderis, Y., Donnadieu, Y., Labat, D., Roelandt, C., 2012. High sensitivity of the continental-weathering carbon dioxide sink to future climate change. Nat. Clim Change 2, 346–349. https://doi.org/10.1038/nclimate1419

9. Binet, S., Joigneaux, E., Pauwels, H., Albéric, P., Fléhoc, C., Bruand, A., 2017. Water exchange, mixing and transient storage between a saturated karstic conduit and the surrounding aquifer: Groundwater flow modeling and inputs from stable water isotopes. J. Hydrol. 544, 278–289. https://doi.org/10.1016/j.jhydrol.2016.11.042

10. Binet, S., Mudry, J., Bertrand, C., Guglielmi, Y., Cova, R., 2006. Estimation of quantitative descriptors of northeastern Mediterranean karst behavior: multiparametric study and local validation of the Siou-Blanc massif (Toulon, France). Hydrogeol. J. 14, 1107–1121. https://doi.org/10.1007/s10040-006-0044-1

11. Binet, S., Spadini, L., Bertrand, C., Guglielmi, Y., Mudry, J., Scavia, C., 2009. Variability of the groundwater sulfate concentration in fractured rock slopes: a tool to identify active unstable areas. Hydrol. Earth Syst. Sci. 13, 2315–2327. www.hydrol-earth-syst-sci.net/13/2315/2009/

12. Bloor J. M.G. and Bardgett R. D. 2012. Stability of above-ground and below-ground processes to extreme drought in model grassland ecosystems: Interactions with plant species diversity and soil nitrogen availability. Perspectives in Plant Ecology, Evolution and Systematics 14 (2012) 193–204

13. Bobbink, R., Heil, G. W., & Raessen, M. B. (1992). Atmospheric deposition and canopy exchange processes in heathland ecosystems. *Environmental pollution*, *75*(1), 29-37.

14. Bond-Lamberty, B., Thomson, A., 2010. Temperature-associated increases in the global soil respiration record. Nature 464, 579.

15. Bouzigues, R., Ribolzi, O., Favrot, J.C., Valles, V., 1997. Carbonate redistribution and hydrogeochemical processes in two calcareous soils with groundwater in a Mediterranean environment. Eur. J. Soil Sci. 48, 201–211. https://doi.org/10.1111/j.1365-2389.1997.tb00541.x

16. Brunet, F., Potot, C., Probst, A., & Probst, J. L. (2011). Stable carbon isotope evidence for nitrogenous fertilizer impact on carbonate weathering in a small agricultural watershed. *Rapid Communications in Mass Spectrometry*, *25*(19), 2682-2690.

17. Caetano Bicalho, C., Batiot-Guilhe, C., Seidel, J.L., Van Exter, S., Jourde, H., 2012. Geochemical evidence of water source characterization and hydrodynamic responses in a karst aquifer. J. Hydrol. 450, 206–218. https://doi.org/10.1016/j.jhydrol.2012.04.059

18. Calmels, D., Gaillardet, J., François, L., 2014. Sensitivity of carbonate weathering to soil CO2 production by biological activity along a temperate climate transect. Chem. Geol. 390, 74–86. https://doi.org/10.1016/j.chemgeo.2014.10.010

19. Charlier J.-B., B. Ladouche, and J.-C. Maréchal, 2015. Identifying the impact of climate and anthropic pressures on karst aquifers using wavelet analysis. Journal of Hydrology, 523:610-623, https://doi.org/10.1016/j.jhydrol.2015.02.003

20. Charmoille, A., Binet, S., Bertrand, C. et al. (2009) Hydraulic interactions between fractures and bedding planes in a carbonate aquifer studied by means of experimentally induced water-table fluctuations (Coaraze experimental site, southeastern France) Hydrogeol J 17: 1607. https://doi.org/10.1007/s10040-009-0470-y

21. Chen, Z., Auler, A.S., Bakalowicz, M., Drew, D., Griger, F., Hartmann, J., Jiang, G., Moosdorf, N., Richts, A., Stevanovic, Z., Veni, G., Goldscheider, N., 2017. The World Karst Aquifer Mapping project: concept, mapping procedure and map of Europe. Hydrogeol. J. 25, 771–785. https://doi.org/10.1007/s10040-016-1519-3

22. Chery, J.L., 1983. Etude hydrochimique d'un aquifère karstique alimenté par perte de cours d'eau (La Loire): Le système des calcaires de Beauce sous le Val d'Orléans (PhD thesis). University of Orléans, Orléans, France.

23. Donnini, M., Frondini, F., Probst, J.-L., Probst, A., Cardellini, C., Marchesini, I., Guzzetti, F., 2016. Chemical weathering and consumption of atmospheric carbon dioxide in the Alpine region. Glob. Planet. Change 136, 65–81. https://doi.org/10.1016/j.gloplacha.2015.10.017

24. Drever, J.I., 1997. The geochemistry of natural waters, Surface and Groundwater Environments, Third edition Prentice-Hall, Upper Saddle River, NJ (436 pp.).

25. Ek, C., Godissart, J., 2014. Carbon dioxide in cave air and soil air in some karstic areas of Belgium. Geol. Belg.

26. Emblanch, C., 1997. Les équilibres chimiques et isotopiques du carbone dans les aquifères karstiques : étude en région méditerranéenne de montagne. Université d'Avignon et Pays de Vaucluse.

27. Emblanch, C., Zuppi, G.., Mudry, J., Blavoux, B., Batiot, C., 2003. Carbon 13 of TDIC to quantify the role of the unsaturated zone: the example of the Vaucluse karst systems (Southeastern France). J. Hydrol. 279, 262–274. https://doi.org/10.1016/S0022-1694(03)00180-X

28. Fleury, P., Ladouche, B., Conroux, Y., Jourde, H., Dörfliger, N., 2009. Modelling the hydrologic functions of a karst aquifer under active water management – The Lez spring. J. Hydrol. 365, 235–243. https://doi.org/10.1016/j.jhydrol.2008.11.037

29. Fleury, P., Plagnes, V., Bakalowicz, M., 2007. Modelling of the functioning of karst aquifers with a reservoir model: Application to Fontaine de Vaucluse (South of France). J. Hydrol. 345, 38–49. https://doi.org/10.1016/j.jhydrol.2007.07.014

30. Gaillardet J. Calmels D., Romero-Mujalli, Zakharova, E., Hartmann J. (2018) Global climate control on carbonate weathering intensity. Chemical Geology. https://doi.org/10.1016/j.chemgeo.2018.05.009

31. Genty D., Blamart D., Ouahdi R., Gilmour M., Baker, 2003 Precise dating of Dansgaard-Oeschger climate oscillations in western Europe form stalagmite data. Nature, 421(6925), 833. https://doi.org/10.1038/nature01391

32. Godsey, S.E., Kirchner, J.W., Clow, D.W., 2009. Concentration–discharge relationships reflect chemostatic characteristics of US catchments. Hydrol. Process. 23, 1844–1864. https://doi.org/10.1002/hyp.7315

33. Gombert, P., 2002. Role of karstic dissolution in global carbon cycle. Global and Planetary Change 33, 177–184. https://doi.org/10.1016/S0921-8181(02)00069-3

34. Huebsch, M., Fenton, O., Horan, B., Hennessy, D., Richards, K. G., Jordan, P., Goldscheider N., Butscher C. and Blum, P. (2014). Mobilisation or dilution? Nitrate response of karst springs to high rainfall events. Hydrol. Earth Syst. Sci., 18, 4423–4435

35. James, E. W., Banner, J. L., and Hardt, B. (2015), A global model for cave ventilation and seasonal bias in speleothem paleoclimate records, Geochem. Geophys. Geosyst., 16, 1044–1051, https://doi.org/10.1002/2014GC005658

36. Jeannin, P.-Y., Hessenauer, M., Malard, A., Chapuis, V., 2016. Impact of global change on karst groundwater mineralization in the Jura Mountains. Sci. Total Environ. 541, 1208–1221. https://doi.org/10.1016/j.scitotenv.2015.10.008

37. Jones, J., Mulholland, P.J., 1998. Carbon Dioxide Variation in a Hardwood Forest Stream: An Integrative Measure of Whole Catchment Soil Respiration. Ecosystems 1, 183–196.

38. Jourde et al. 2018 SNO KARST: a French network of observatories for the multidisciplinary study of critical zone processes in karst watersheds and aquifers Vadoze zone journal on line.

39. Quinif, Y., Baele, J. M., Dubois, C., Havron, C., Kaufmann, O., Vergari, A. (2014). Fantômisation: un nouveau paradigme entre la théorie des deux phases de Davis et la théorie de la biorhexistasie d'Erhart. Geologica Belgica.

40. Ladouche, B., Maréchal, J.-C., Dörfliger, N., 2014. Semi-distributed lumped model of a karst system under active management. J. Hydrol. 509, 215–230.

41. Liu and Zhao, 1999. Contribution of carbonate rock weathering to the atmospheric CO2 sink. Environmental Geology 39: 1053-1058

42. Liu, Z., Zhao, J., 2000. Contribution of carbonate rock weathering to the atmospheric CO2 sink. Environ. Geol. 39, 1053–1058. https://doi.org/10.1007/s002549900072

43. Mangin, A., 1984. Pour une meilleure connaissance des systèmes hydrologiques à partir des analyses corrélatoire et spectrale. J. Hydrol. 67, 25–43. https://doi.org/10.1016/0022-1694(84)90230-0

44. Marjolet, G., Salado, J., 1978. Le système karstique de la source du Lez (Hérault). Méditerranée 71–83.

45. Moncoulon, D., Probst, A., & Martinson, L. (2007). Modeling acidification recovery on threatened ecosystems: application to the evaluation of the Gothenburg protocol in France. *Water, Air, & Soil Pollution: Focus*, *7*(1-3), 307-316.

46. Monnin, M., Seidel, J.L., Bakalowicz, M., 1998. The Baget karst system, Final report on the KATRIN project.

47. Mudarra, M., & Andreo, B. (2010). Hydrogeological functioning of a karst aquifer deduced from hydrochemical components and natural organic tracers present in spring waters. The case of Yedra Spring (Southern Spain). *Acta Carsologica*, *39*(2).

48. Mudry, J., 1987. Apport du traçage physico-chimique naturel à la connaissance hydrocinématique des aquifères carbonatés. Université de Franche-Comté.

49. Parkhurst, D.L., Appelo, C.A.J., 1999. User's guide to PHREEQC (Version 2): A computer program for speciation, batch-reaction, one-dimensional transport, and inverse geochemical calculations.

50. Pascaud, A., Sauvage, S., Coddeville, P., Nicolas, M., Croisé, L., Mezdour, A., Probst, A., 2016. Contrasted spatial and long-term trends in precipitation chemistry and deposition fluxes at rural stations in France. Atmos. Environ. 146, 28–43. https://doi.org/10.1016/j.atmosenv.2016.05.019

51. Perrin, A.-S., Probst, A., Probst, J.-L., 2008. Impact of nitrogenous fertilizers on carbonate dissolution in small agricultural catchments: Implications for weathering CO2 uptake at regional and global scales. Geochim. Cosmochim. Acta 72, 3105–3123. https://doi.org/10.1016/j.gca.2008.04.011

52. Perrin, J., Jeannin, P. Y., & Zwahlen, F. (2003). Implications of the spatial variability of infiltration-water chemistry for the investigation of a karst aquifer: a field study at Milandre test site, Swiss Jura. *Hydrogeology Journal*, *11*(6), 673-686.

53. Peyraube, N., 2011. Apports des équilibres calco-carboniques et du carbone 13 pour l'étude de l'air et des écoulements d'eau dans la zone non saturée du karst: application au système karstique perché de la grotte de Cussac (Dordogne, France). Bordeaux 1.

54. Peyraube, N., Lastennet, R., Denis, A., 2012. Geochemical evolution of groundwater in the unsaturated zone of a karstic massif, using the PCO2–SIc relationship. J. Hydrol. 430, 13–24. https://doi.org/10.1016/j.jhydrol.2012.01.033

55. Peyraube, N., Lastennet, R., Denis, A., Malaurent, P., 2013. Estimation of epikarst air PCO2 using measurements of water δ13CTDIC, cave air PCO2 and δ13CCO2. Geochimica et Cosmochimica Acta 118, 1–17. https://doi.org/10.1016/j.gca.2013.03.046

56. Peyraube, N., Lastennet, R., Denis, A., Minvielle, S., Houillon, N., Lorette, G , Denimal S., Bertrand C., Binet S., Emblanch, C., Villanueva J. D. (2019). SIc–Abacus: An in–situ tool for estimating SIc and Pco2 in the context of carbonate karst. Journal of Hydrology, 568, 891-903

57. Probst, A., Dambrine, E., Viville, D., Fritz, B., 1990. Influence of acid atmospheric inputs on surface water chemistry and mineral fluxes in a declining spruce stand within a small granitic catchment (Vosges Massif, France). Transf. Elem. Hydrol. Cycle 116, 101–124. https://doi.org/10.1016/0022-1694(90)90118-H

58. Probst, A., Lelong, F., Viville, D., Durand, P., Ambroise, B., Fritz, B., 1995. Comparative Hydrochemical Behaviour and Element Budgets of the Aubure (Vosges Massif) and Mont-Lozère (Southern Massif Central) Norway Spruce Forested Catchments, in: Landmann, G., Bonneau, M., Kaennel, M. (Eds.), Forest Decline and Atmospheric Deposition Effects in the French Mountains. Springer Berlin Heidelberg, pp. 203–225.

59. Probst, A., Party, J.P., Fevrier, C., Dambrine, E., Thomas, A.L., Stussi, J.M., 1999. Evidence of springwater Acidification in the Vosges Mountains (North-East of France): Influence of Bedrock Buffering Capacity. Water. Air. Soil Pollut. 114, 395–411. https://doi.org/10.1023/A:1005156615921

60. Raich, J.W., Tufekciogul, A., 2000. Vegetation and soil respiration: correlations and controls. Biogeochemistry 48, 71–90.

61. Raymond, P.A., Oh, N.-H., Turner, R.E., Broussard, W., 2008. Anthropogenically enhanced fluxes of water and carbon from the Mississippi River. Nature 451, 449–452. https://doi.org/10.1038/nature06505

62. Schöpp, W., Posch, M., Mylona, S., & Johansson, M. (2003). Long-term development of acid deposition (1880? 2030) in sensitive freshwater regions in Europe. Hydrology and Earth System Sciences, 7(4), 436-446.

63. Stets, E.G., Kelly, V.J., Crawford, C.G., 2014. Long-term trends in alkalinity in large rivers of the conterminous US in relation to acidification, agriculture, and hydrologic modification. Sci. Total Environ. 488–489, 280–289. https://doi.org/10.1016/j.scitotenv.2014.04.054

64. Szczypta, C., Gascoin, S., Houet, T., Hagolle, O., Dejoux, J.-F., Vigneau, C., Fanise, P., 2015. Impact of climate and land cover changes on snow cover in a small Pyrenean catchment. J. Hydrol. 521, 84–99. https://doi.org/10.1016/j.jhydrol.2014.11.060

65. White, W.B., 1999. Geomorphology and Hydrology of Karst Terrains. Oxford University Press.

66. Wright, R., 1983. Predicting acidification of North American lakes (Research Report No. NIVA-rapport;1477). Norsk institutt for vannforskning.

LISTE OF TABLES

Table 1 : Location and hydro-climatological characteristics of the 5 karst hydrosystems. pCO$_2$ values come from previous studies

Table 2: Average and standard deviation (in italics) of air temperature, concentrations (in brackets) and fluxes (F) for the 5 sites studied. A and N refer to natural and anthropogenic source, respectively (according to eq. 5, 8, 9, see text)

Table 3: annual average values for HCO$_3$, Ca+Mg observed at the 5 karst springs studied. [Ca+Mg]$_A$ and [Ca+Mg]$_N$ are respectively the amount of [Ca+Mg] produced by anthropogenic dissolution due to strong acids (A) and by natural dissolution due to carbonic acid (N), as calculated following eq.9. ISc and ISd are the calculated saturation index vs. calcite and dolomite, respectively, determined using PhreeqC software. The sample number is the one used to calculate the average for each year. dep_sum is the sum of S+N atmospheric deposits for each site as estimated by Schöpp et al. (2003). A 0.3 ratio was applied on the VdO flux estimation to take initial river composition into account. Values in italics are inter-annual averages used to fill the gaps in the dataset

Table 4: Parameters characteristics of the relationship between [Ca+Mg]$_A$ fluxes and the sum of atmospheric H+ deposition (dep_sum) for all the studied sites (first line), and then excluding one site after the other to test the robustness of the linear relationship. An average and a standard deviation of the regression coefficients can be estimated.

Table 5: Parameters of the linear regression between annual fluxes and air temperature considering the sites in different ways. The slope, ordinate at origin, Pearson correlation coefficients, sample numbers and p values are given for an analysis on the entire dataset, and then excluding one study site after the other. This exclusion test makes it possible to calculate an average value and a standard deviation.

LISTE OF FIGURES

Figure 1 : Location of the five selected karst hydrosystems on the west European map of continuous (dark grey) and discontinuous (grey) carbonate rocks (Chen et al., 2017)

Figure 2: Long-term monitoring data set of Ca+Mg and HCO$_3$ concentrations (in mmol.L^{-1}) and of mean daily discharge (Q in m^3.s^{-1}) for the Baget spring.

Figure 3: Monthly average concentrations of [HCO$_3$] vs [Ca+Mg] over the period studied for each of the 5 sites. Theoretical 1:1 and 1:2 lines correspond to anthropogenic (strong acids) and natural (carbonic acid) carbonate dissolution, respectively.

Figure 4 : Monthly average concentrations of [Mg] vs[Ca+Mg]$_A$ in karst discharge water over the studied period for each of the 5 sites.

Figure 5: Relationships between annual average concentrations of [Ca, Mg]$_N$ and air temperature for the 5 karst hydrosystems. Each black line represents the theoretical evolution of [Ca, Mg]$_N$ derived from equation 10 for a given air temperature and pCO$_2$ (atm).

Figure 6: Annual total proton deposition vs [Ca+Mg] $_A$. Dashed line is the linear regression with all the datasets. The labels show the sampled year. Point without year label are all comprised between 1995 and 2005.

Figure.7: Relationship between annual flux of [Ca, Mg]$_N$ calculated for an average discharge and air temperature. Grey lines are error bars, dashed line is the linear regression, dotted lines are the linear regressions with the maximum and the minimum slopes calculated inside the error bars.

Figure 8: Interannual fluctuations at the Baget site of average monthly values A/ annual histogram of atmospheric deposition (dep_sum) and sulfates in open field precipitation B/ : water discharge C/ air temperature, D/ [Ca+ Mg]$_A$ and E/ [Ca+ Mg]$_N$. Continuous blue lines are the mean monthly values. Black points are the annual averages and black lines are modelled annual values of [Ca+ Mg] $^*_A$ and [Ca+ Mg] $^*_N$ concentrations calculated from the linear regressions involving atmospheric acid deposits (Table 4) and annual air temperature (Table 5), respectively. F/ shows seasonal fluctuation of an average year with standard deviations.

Spring	Lez	Farfal	FdV	Baget	ValdO
Watershed_km^2	130	0.87	1,130	13.25	70
Latitude (°, min, s)	43° 41' 04" N	44° 49' 44'' N	43° 55' 04'' N	42° 57' 20'' N	47° 51' 01" N
Longitude (°, min, s)	3° 50' 50" E	0° 50' 42'' E	5° 07' 58'' E	1° 01' 47'' E	1° 56' 15" E
Elevation (m)	50	200	119	496	93
Sampling period (year):	1975 1997-2009	2008-2009	1981; 1995; 2003-2006	1978-2005	1980; 1994; 2008-2009
Weather station	Montpellier	Gourdon	St Christol	St Girons	Orléans
annual average T_{air} (°C)	14.8	12.6	9.7	10.6	11.0
Discharge (m$^3\cdot$s^{-1})	2.5	0.01	20	0.43	12.5
Sp. discharge (L.m^{-2}.yr^{-1})	604	507	558	1023	5631
Dynamic volume (10^6 m^3)	10	0.03	387	2	21
Average Residence time (yr)	0.13	0.07	0.61	0.15	0.05
Summer pCO_2 (atm)	$10^{-1.5}$	$10^{-1.5}$	$10^{-1.8}$	$10^{-1.9}$	/
Winter pCO_2 (atm)	$10^{-1.4}$	$10^{-2.6}$	$10^{-2.2}$	$10^{-2.6}$	/

33

Parameters	Units	Lez		Farfal		FdV		Baget		ValdO	
		Avg	StD	Avg	StD	Avg	StD	Avg	StD	Avg	StD
Air_Temp	°C	14.7	*6.1*	13.0	*6.2*	9.2	*6.0*	10.4	*3.9*	11.3	*5.4*
[HCO3]	mmol.L^{-1}	5.92	*0.20*	5.51	*0.11*	4.08	*0.29*	2.89	*0.19*	1.98	*0.18*
[Mg]	mmol.L^{-2}	0.36	*0.05*	0.11	*0.01*	0.24	*0.06*	0.37	*0.05*	0.16	*0.04*
[Ca+Mg]	mmol.L^{-1}	3.36	*0.67*	2.99	*0.04*	2.34	*0.26*	1.67	*0.10*	1.12	*0.10*
[Ca+Mg]$_A$	mmol.L^{-1}	0.79	*0.22*	0.47	*0.12*	0.60	*0.56*	0.46	*0.13*	0.29	*0.20*
[Ca+Mg]$_N$	mmol.L^{-1}	2.57	*0.16*	2.52	*0.11*	1.74	*0.37*	1.22	*0.13*	0.84	*0.16*
%[Ca+Mg]$_A$	%	24		16		26		27		25	
F$_{[HCO3]}$	mol.m^{-2}.year^{-1}	3.5	*0.7*	1.3	*1.77*	1.6	*1.24*	3.0	*2.7*	2.2	*1.3*
F$_{[Ca+Mg]A}$	mol.m^{-2}.year^{-1}	0.47	*0.8*	0.10	*0.13*	0.21	*0.21*	0.39	*0.3*	0.27	*0.3*
F$_{[Ca+Mg]N}$	mol.m^{-2}.year^{-1}	1.53	*0.9*	0.58	*0.82*	0.72	*0.57*	1.30	*1.2*	0.94	*0.6*

Site	Year	T_{air} °C	Temp_water_ °C	Q L.m⁻².year⁻¹	dep_sum (V2006) eq.m⁻².yr⁻¹	pH	Ca+Mg mmol.L⁻¹	HCO3 mmol.L⁻¹	$[Ca+Mg]_A$ mmol.L⁻¹	$[Ca+Mg]_N$ mmol.L⁻¹	SO4_rain mmol.L⁻¹	% $[Ca+Mg]_A$	Isc	Isd	$F[Ca+Mg]_A$ mol.m⁻².yr⁻¹	$F[Ca+Mg]_N$ mol.m⁻².yr⁻¹	sample Nb
Lez	1975	*13.0*		*604*	0.25		3.09	5.49	0.69	2.40		22			0.42	1.5	130
Lez	1997	15.5	14.9	*604*	0.12	7.1	3.29	5.84	0.74	2.55		23	0.1	-0.8	0.45	1.5	4
Lez	1998	16.5	16.3	*604*	0.09	7.1	3.40	5.98	0.83	2.57		24	0.2	-0.5	0.50	1.6	6
Lez	1999	16.1	16.4	*604*	0.09	7.2	3.27	5.73	0.80	2.47		24	0.2	-0.5	0.48	1.5	8
Lez	2000	16.1	15.3	*604*	0.15	7.2	3.14	5.73	0.55	2.59		17	0.2	-0.5	0.33	1.6	2
Lez	2001	16.8	16.5	*604*	0.14	7.1	3.33	5.97	0.69	2.64		21	0.1	-0.6	0.42	1.6	10
Lez	2002	17.7	16.9	*604*	0.14	7.2	3.48	6.04	0.93	2.55		27	0.2	-0.4	0.56	1.5	8
Lez	2003	16.5	17.5	*604*	0.15	7.0	3.36	6.00	0.71	2.64		21	0.1	-0.8	0.43	1.6	8
Lez	2004	15.1	15.1	*604*	0.13	7.4	3.36	5.97	0.75	2.61		22	0.6	0.4	0.45	1.6	10

Lez	2005	16.0	15.7	*604*	0.12	7.5	3.39	6.03	0.75	2.64		22	0.5	0.2	0.46	1.6	12
Lez	2006	15.4	16.4	*604*	0.15	7.3	3.35	5.93	0.77	2.58		23	0.3	-0.2	0.47	1.6	12
Lez	2007	15.6	16.0	*604*	0.10	7.2	3.49	6.08	0.90	2.59		26	0.2	-0.4	0.54	1.6	4
Lez	2008	15.4	14.1	*604*	0.12	7.2	3.44	5.94	0.95	2.49		28	0.2	-0.4	0.57	1.5	36
Lez	2009	14.1	15.5	*604*	0.08	7.2	3.34	5.94	0.75	2.59		22	0.2	-0.5	0.45	1.6	36
Farfal	2008	12.6	12.5	507	0.05	7.1	2.99	5.57	0.40	2.59		13	0.0	-1.1	0.20	1.3	25
Farfal	2009	13.0	12.6	507	0.04	7.2	2.92	5.35	0.50	2.43		17	0.0	-1.2	0.25	1.2	26
Baget	1979	9.8		1270		7.6	1.62	2.75	0.49	1.13		30			0.51	1.2	52
Baget	1980	9.7	9.4	1270	0.23	7.6	1.62	2.85	0.40	1.22		24			0.41	1.3	49
Baget	1981	10.8		1383		7.7	1.58	2.77	0.40	1.18		25			0.41	1.2	52
Baget	1982	10.4		1315		7.6	1.63	2.83	0.42	1.21		26	0.1	-0.1	0.43	1.2	52
Baget	1983	10.5	10.3	756		7.7	1.64	2.85	0.43	1.21		26			0.44	1.2	52
Baget	1984	9.9		1325		7.6	1.65	2.83	0.46	1.18		28	0.2	-0.1	0.47	1.2	56
Baget	1985	10.2		923	0.21	7.7	1.62	2.72	0.52	1.10		32	0.2	0.1	0.54	1.1	53

Name	Year																
Baget	1986	10.0		1080		7.7	1.61	2.69	0.54	1.08	0.03	33			0.55	1.1	51
Baget	1987	10.6	9.8	868		7.7	1.63	2.80	0.45	1.18		28			0.46	1.2	53
Baget	1988	11.0		*1023*		7.6	1.64	2.83	0.46	1.18		28			0.47	1.2	52
Baget	1989	10.4	10.2	*1023*		7.7	1.69	2.83	0.54	1.14		32			0.55	1.2	74
Baget	1991	9.8	10.0	1023	0.17	7.5	1.67	2.87	0.47	1.20		28			0.48	1.2	52
Baget	1992	10.1	10.1	1506		7.5	1.68	2.90	0.45	1.23		27			0.46	1.3	54
Baget	1993	10.7	10.1	882		7.4	1.70	2.92	0.48	1.22		28			0.49	1.2	53
Baget	1994	10.5	10.0	1353		7.5	1.66	2.86	0.46	1.20	0.05	28			0.47	1.2	52
Baget	1995	10.5	10.1	1153	0.13	7.6	1.69	2.91	0.46	1.23	0.04	27	0.2	0.0	0.47	1.3	53
Baget	1996	11.1	10.1	1239	0.14	7.6	1.73	3.02	0.44	1.29	0.04	25	0.3	0.1	0.45	1.3	52
Baget	1997	10.1	9.6	523	0.13	7.6	1.74	2.96	0.53	1.22	0.03	30	0.2	0.0	0.54	1.2	45
Baget	1998	10.5		956	0.12	7.6	1.75	3.02	0.47	1.28	0.03	27	0.2	0.0	0.48	1.3	50
Baget	1999	10.8		958	0.13	7.7	1.70	2.97	0.43	1.27	0.05	25	0.3	0.1	0.44	1.3	52
Baget	2000	10.1		795	0.10	7.7	1.73	3.05	0.42	1.31	0.05	24	0.3	0.2	0.43	1.3	50
Baget	2001	11.6		946	0.10	7.8	1.71	3.03	0.38	1.32	0.04	23	0.4	0.4	0.39	1.4	49
Baget	2002	10.7		1204	0.10	7.7	1.74	3.10	0.38	1.36	0.03	22	0.3	0.2	0.39	1.4	47
Baget	2003	10.2		969	0.10	7.7	1.70	2.96	0.44	1.26	0.03	26	0.3	0.2	0.45	1.3	52
Baget	2004	11.3		1101	0.10	7.7	1.63	2.82	0.45	1.18	0.03	27	0.3	0.0	0.46	1.2	50

Baget	2005	11.7		*1074*	0.10	7.6	1.68	2.95	0.40	1.27	0.04	24	0.2	-0.1	0.41	1.3	50
Vald O	1975	10.1		*5631*	0.32		*1.13*	*1.87*	0.39	0.74		35		-0.1	*0.66*	*1.3*	5
Vald O	1980	11.0	12.7	*5631*	0.32	7.8	*1.12*	*1.84*	0.40	0.72		36	-0.1	-0.9	*0.68*	*1.2*	34
Vald O	1994	11.3	12.8	*5631*	0.14	7.8	*1.11*	*1.89*	0.33	0.78		30	-0.1	-0.9	*0.56*	*1.3*	14
Vald O	2009	12.3	13.3	*5631*	0.04	7.8	*1.12*	*2.08*	0.15	0.96		14	-0.2	-0.9	*0.26*	*1.6*	13
FdV	1981	9.0	12.6	615		7.4	2.13	3.97	0.30	1.83		14	0.0	-1.0	0.17	1.0	56
FdV	1995	10.1	12.8	549	0.05	7.2	2.41	4.32	0.51	1.91		21	0.0	-1.0	0.28	1.1	118
FdV	2004	9.6	12.6	328	0.07	7.2	2.32	4.23	0.41	1.91		18	-0.1	-1.2	0.23	1.1	45
FdV	2005	9.2	12.4	215	0.07	7.1	2.25	4.24	0.27	1.99		12	-0.2	-1.4	0.15	1.1	44
FdV	2006	10.7	12.6	244	0.06	7.1	2.52	4.01	1.02	1.49		4	-0.1	-1.3	0.57	0.8	21

F[Ca+Mg]A = f(Dep_sum)

Sites	a	b	r²	n	p_value
Lez, Farfal, Baget, FdV, ValdO	1.12	0.31	0.35	51	<0.001
Farfal, Baget, FdV, ValdO	1.19	0.28	0.49	36	<0.001
Lez, Baget, FdV, ValdO	0.95	0.33	0.55	49	<0.001
Lez, Farfal, FdV, ValdO	1.29	0.28	0.42	24	<0.001
Lez, Farfal, Baget, ValdO	0.86	0.35	0.56	46	<0.001
Lez, Farfal, Baget, FdV	0.89	0.33	0.35	46	<0.001
Average :	1.05	0.31	0.45		
StD :	0.18	0.03	0.09		

$F_{[Ca+Mg]N} = f(T_{air})$

Sites	a	b	r²	n	p_value
Lez, Farfal, Baget, FdV, ValdO	0.061	0.58	0.74	51	<0.001
Farfal, Baget, FdV, ValdO	0.055	0.64	0.29	36	<0.001
Lez, Baget, FdV, ValdO	0.062	0.58	0.75	49	<0.001
Lez, Farfal, FdV, ValdO	0.072	0.41	0.80	25	<0.001
Lez, Farfal, Baget, ValdO	0.055	0.67	0.83	46	<0.001
Lez, Farfal, Baget, FdV	0.062	0.57	0.76	46	<0.001
Average :	0.061	0.57	0.69		
StD :	0.006	0.09	0.20		

Figure 1
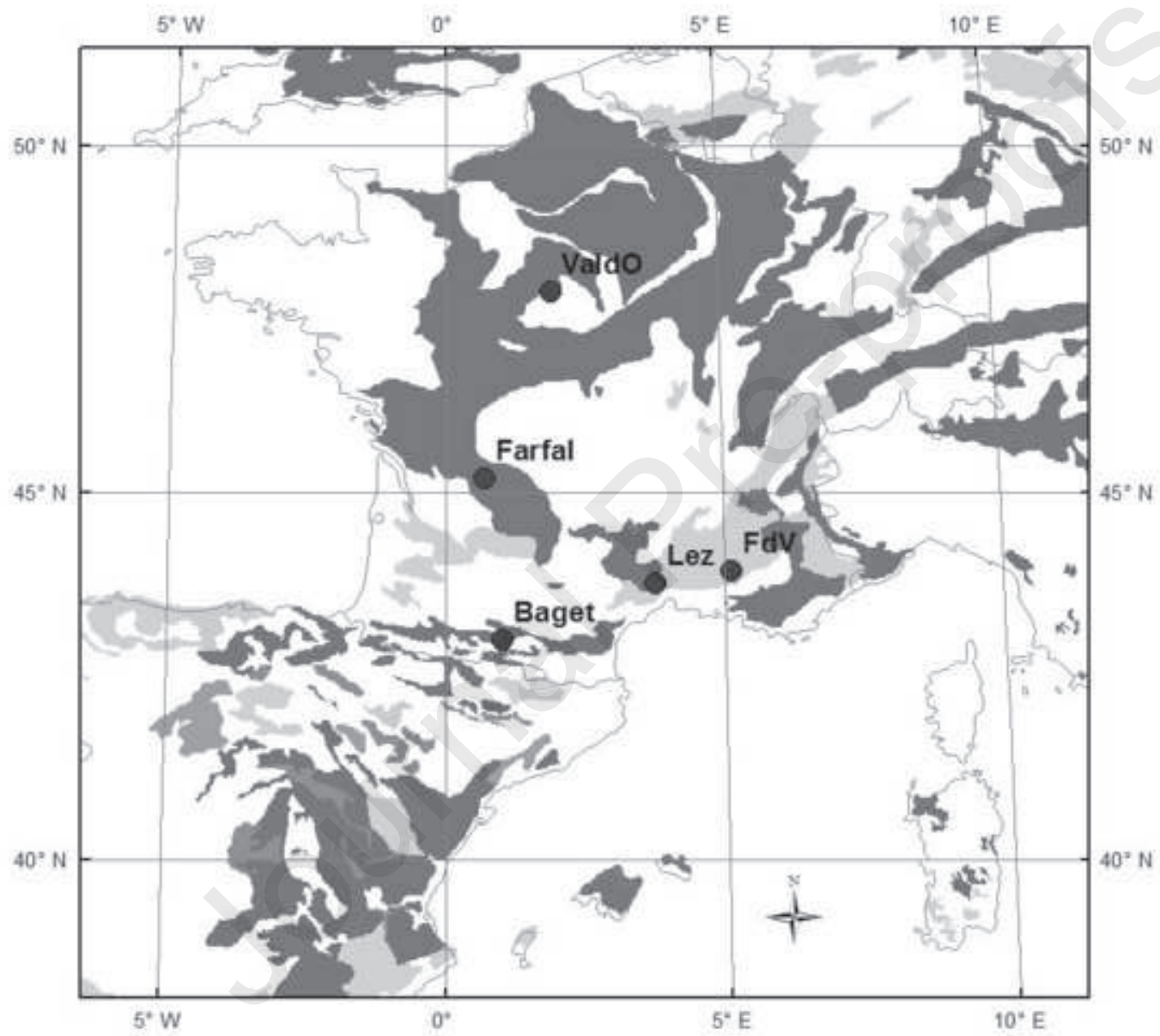
Figure 2
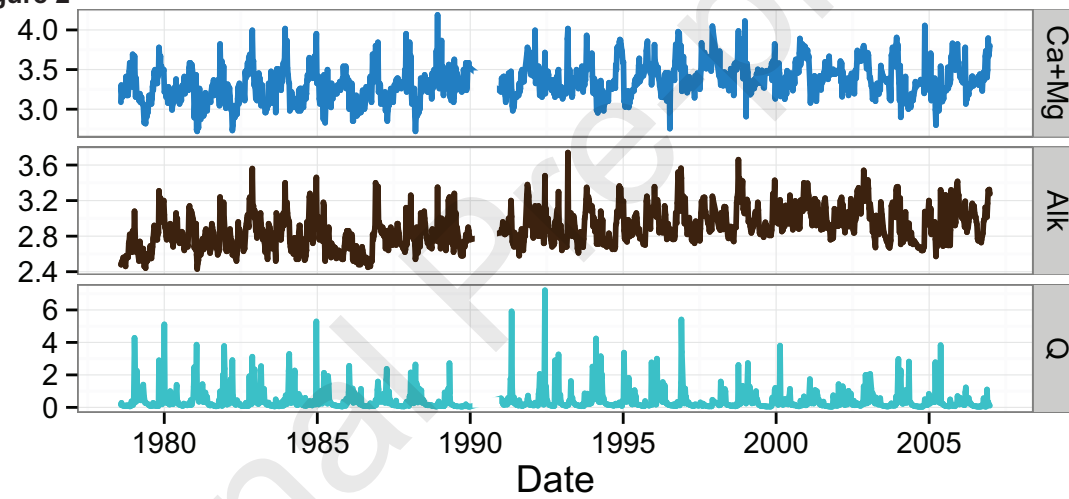
Figure 3
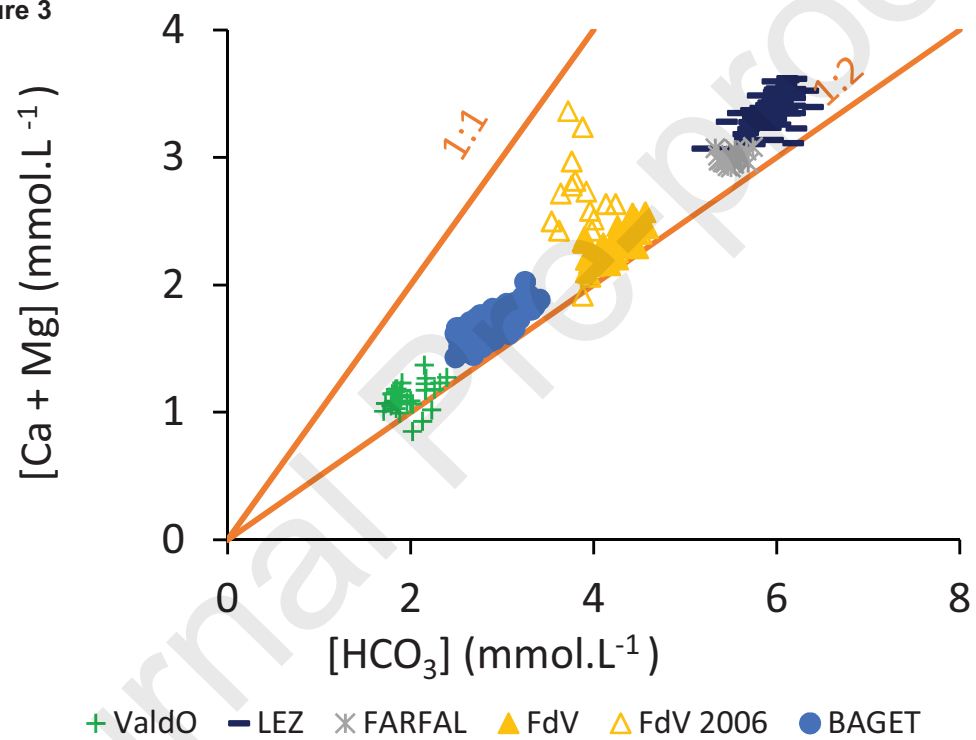
Figure 4

Figure 5

Figure 6

F[Ca+Mg]$_A$ (mol.m^{-2}.yr^{-1})

dep_sum (mol.m^{-2}.yr^{-1})

1:1

2007
2008
1994
2006
2009
2002
1997
2006
1991
1985
2000
1980 1975
2009
1995
1980 1975
2004
2008
2005

✳ Farfal   ▲ FdV   △ FdV 2006   ● Baget   ▬ Lez   ✚ ValdO

Figure 7

Legend: Lez, Farfal, FdV, FdV 2006, Baget, ValdO

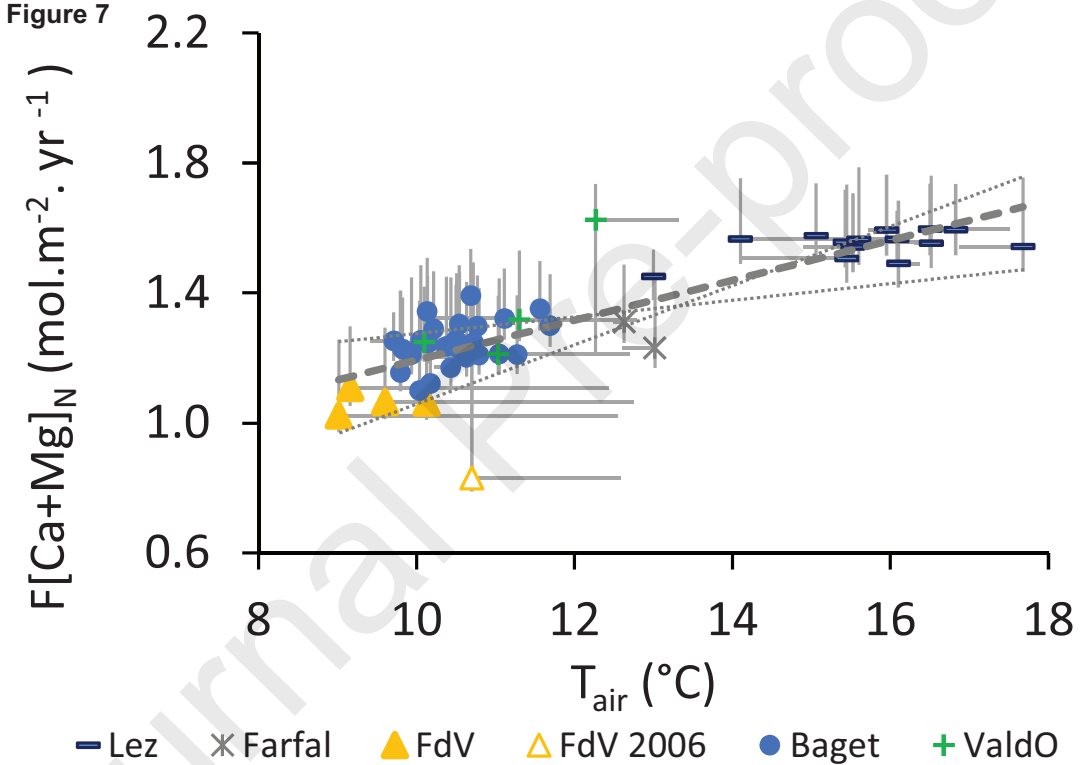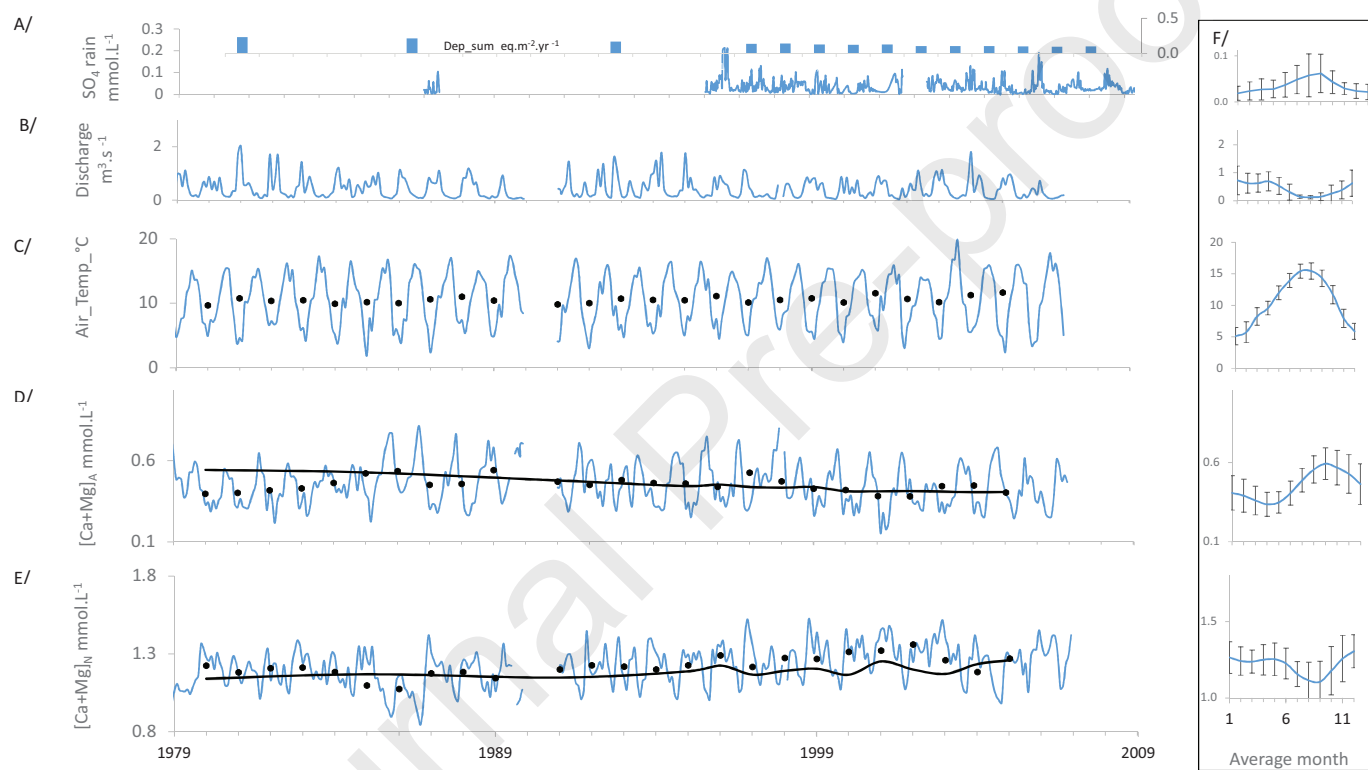Y-axis: F[Ca+Mg]$_N$ (mol.m^{-2}.yr^{-1})

X-axis: T$_{air}$ (°C)
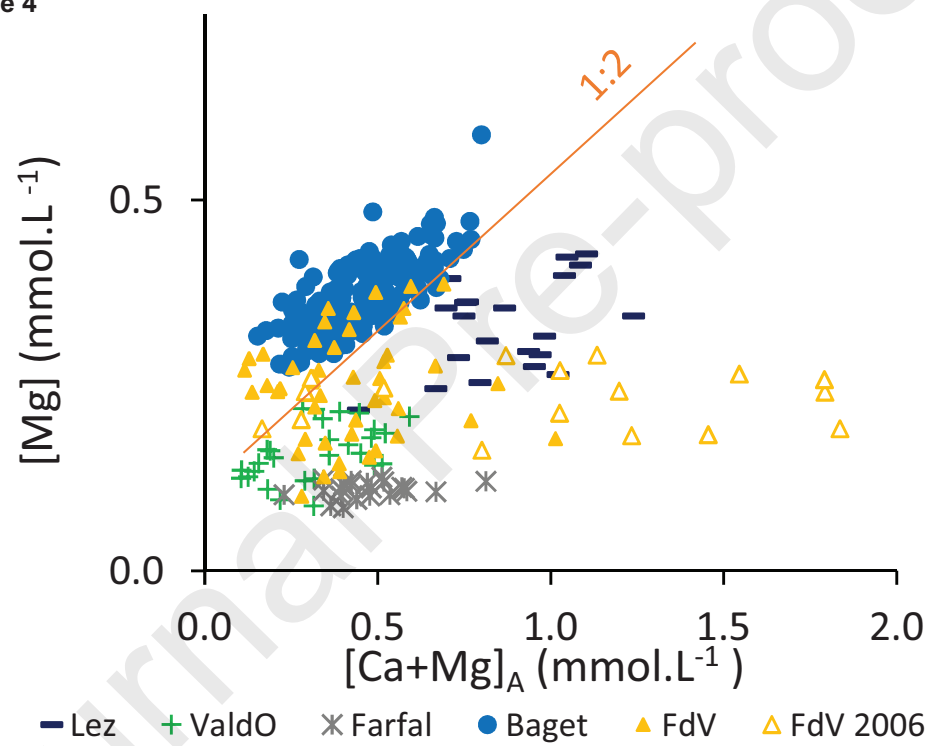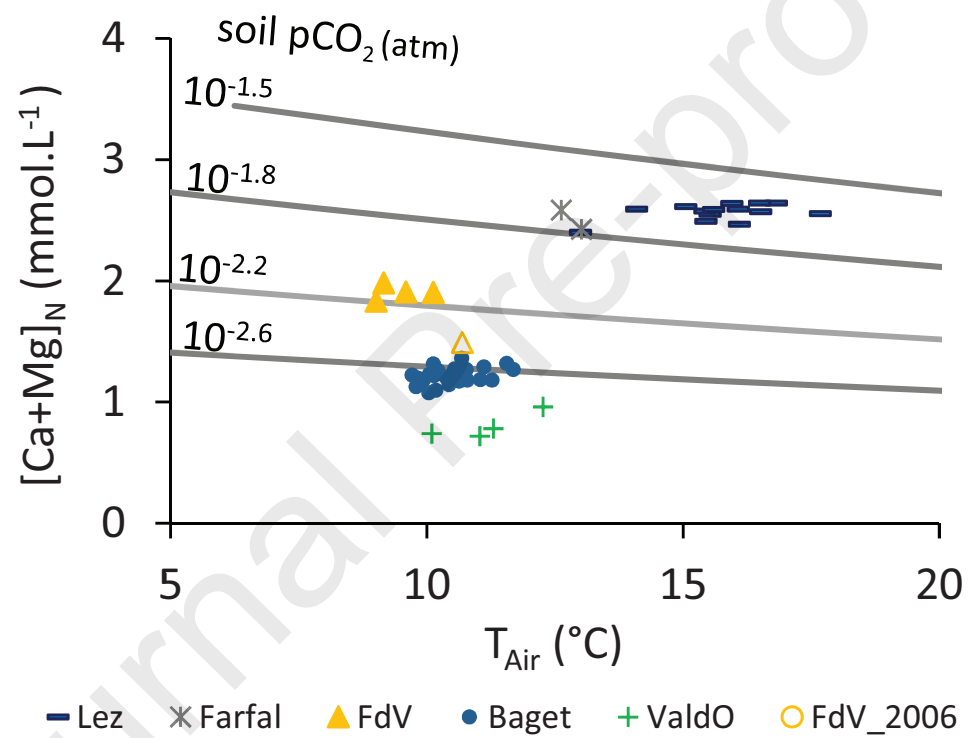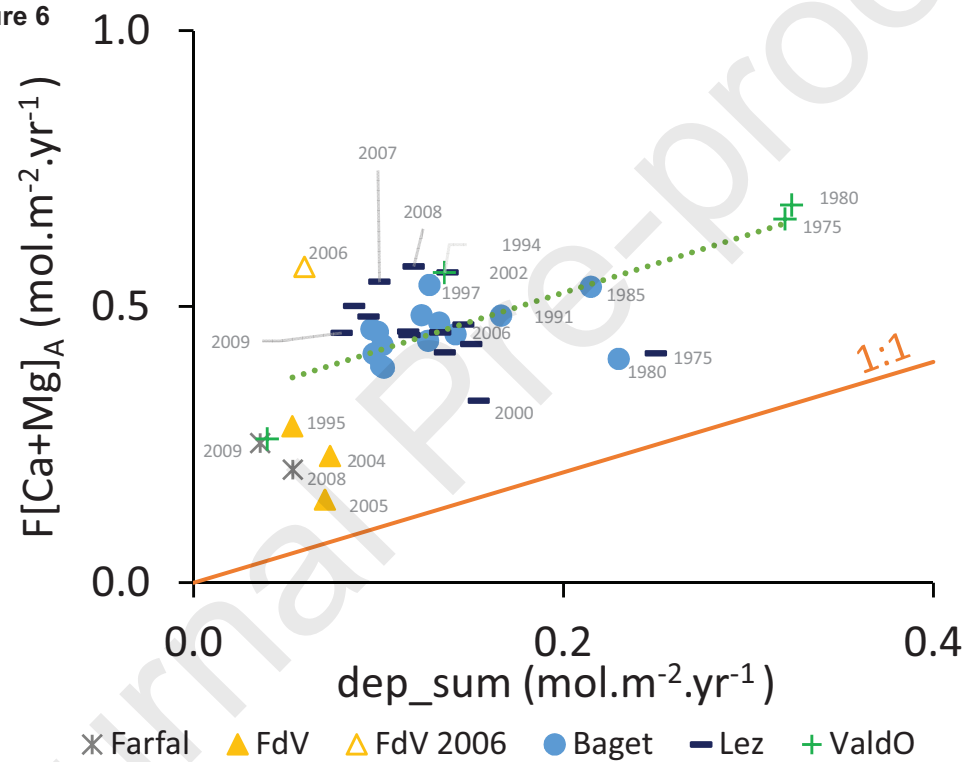
Figure 8

Declaration of interests

☒ The authors declare that they have no known competing financial interests or personal relationships that could have appeared to influence the work reported in this paper.

☐ The authors declare the following financial interests/personal relationships which may be considered as potential competing interests: